OUKA
The University of Osaka
Institutional Knowledge Archive

Title	Analysis of complex spikes of Purkinje cells in the cerebellar ventral paraflocculus during ocular following responses in monkeys
Author(s)	小林, 康
Citation	大阪大学, 1998, 博士論文
Version Type	VoR
URL	https://doi.org/10.11501/3151125
rights	
Note	

The University of Osaka Institutional Knowledge Archive : OUKA

https://ir.library.osaka-u.ac.jp/

The University of Osaka

B7611

Analysis of complex spikes of Purkinje cells in the cerebellar ventral paraflocculus during ocular following responses in monkeys.

Yasushi Kobayashi

Analysis of Complex Spikes of Purkinje Cells in the Cerebellar Ventral Paraflocculus During Ocular Following Responses in Monkeys.

Yasushi Kobayashi

ATR Human Information Processing Research Labs, Kyoto 619-02, Japan

Contents

1 ABSTRACT 6

2 INTRODUCTION 8

2.1 Internal model of controlled object 8

2.2 Inverse model and cerebellum 9

2.3 Visuo-motor signal transformation in the cerebellum 11

2.4 Analysis of firing probability using generalized linear model . . . 13

2.5 Hypotheses about function of complex spike 14

2.6 The VPFL and Ocular Following Responses 17

2.7 Complex spikes in the VPFL 18

2.8 Purpose of the present study 19

3 METHODS 20

3.1 Surgery 20

3.2 Behavioral paradigm 20

3.3 Visual stimuli 21

3.4 Recording technique 23

3.5 Generalized linear model 25

4 RESULTS 31

4.1 Electrical activity of Purkinje cell in the VPFL 31

4.2 Directional tuning of CS 35

4.3 Effects of stimulus velocity on CS and SS 39

4.4 Temporal patterns of CS firing rates 43

4.5 Examination of generalized linear model for firing data 45

4.6 Reproduction of firing probability of CS 54
4.7 Short-term modulation of SS by CS 70
4.8 The movement with or without CS 72

5 DISCUSSION **74**

5.1 The type of information encoded by CS and the mechanism involved 74
5.2 Real-time motor control by CS 79
5.3 Interactions between CS and SS for individual cells 82
5.4 CS may convey information sufficient for motor learning 85

List of Figures

2.1 Two types of internal models 8
2.2 Temporal profile of SS firing rate during OFR 10
2.3 Reconstruction of SS by inverse-dynamics model 12
2.4 Neural substrates related to OFR 13

3.1 Experimental set up 21
3.2 Behavioral paradigm for directional selectivity 22
3.3 Behavioral paradigm for speed tuning 23
3.4 Binomial distribution of spike counts 26
3.5 Sigmoid function 27

4.1 Electrical activity of Purkinje cell in the VPFL 32
4.2 Eye movements and CS and SS during OFR 33
4.3 SS and CS peristimulus histograms in response to moving the stimulus in eight different directions. 35
4.4 Directional tuning properties of SS and CS. 37
4.5 Preferred direction of SS and CS for each cell 38
4.6 SS and CS of an example V cell in response to a wide range of stimulus velocities. 40
4.7 Velocity tuning curves of SS and CS. 41
4.8 Reciprocal relationships between the CS and SS firing rates. . . 44
4.9 Data sampling for confirming the binomial distribution of spike counts 45
4.10 The mean and the variance of spike counts 46
4.11 Auto-correlation in CS and SS 47

4.12 Reconstruction using the minimum squared error method 48
4.13 Comparison of reconstruction between generalized linear model and normal linear model 49
4.14 Residual error in SS and CS 50
4.15 Coefficient of determination in CS and SS 51
4.16 Deviance in SS and CS 52
4.17 Confidence interval of model parameters in SS and CS 53
4.18 Reconstruction of SS and CS by generalized linear model of eye movement for individual cells 55
4.19 Reconstruction of multiple SS and CS data with eye movement model by a single set of parameters 56
4.20 Reconstruction of SS and CS by generalized linear model of eye movement and retinal slip 59
4.21 Reconstruction of SS and CS by generalized linear model of eye movement and retinal slip 62
4.22 The estimated parameters 67
4.23 The cross-correlation analysis of SS and CS 71
4.24 Eye velocity and SS with or without CS 73

List of Tables

4.1 Comparison of deviance values 60
4.2 Comparison of estimated model parameters 64
4.3 The best model composed of eye movement or retinal slip 69

Chapter 1

ABSTRACT

Many theories of cerebellar motor learning propose that complex spikes (CS) provide essential error signals for learning and modulate parallel fiber inputs that generate simple spikes (SS). These theories, however, do not satisfactorily reconcile what modality is represented by CS or how information is conveyed by the ultra-low CS firing rate (1 Hz). To further examine the function of CS and the relationship between CS and SS in the cerebellum, CS and SS were recorded in the ventral paraflocculus (VPFL) of awake monkeys during ocular following responses (OFR). In addition, a new statistical method utilizing a generalized linear model of firing probability based on a binomial distribution of the spike count was developed for analysis of the ultra-low CS firing rate.

The results of the present study showed that the spatial coordinates of CS were aligned with those of SS and the speed-tuning properties of CS and SS were more linear for eye movement than retinal slip velocity, indicating that CS contain a motor component in addition to the sensory component identified in previous studies. The generalized linear model to reproduce firing probability confirmed these results, demonstrating that CS conveyed high frequency information with its ultra-low firing frequency, and conveyed both sensory and motor information. Although the temporal patterns of the CS were similar to those of the SS when the sign was reversed and magnitude was amplified about 50 times, the velocity/acceleration coefficient ratio of eye movement model, an aspect of the CS temporal firing profile, was less than that of the SS, suggesting

that CS were more sensory in nature than SS. A cross-correlation analysis of SS that are triggered by CS revealed that short-term modulation, that is, the brief pause in SS caused by CS, does not account for the reciprocal modulation of SS and CS.

The results also showed that three major aspects of the CS and SS individual cell firing characteristics were negatively correlated on a cell-to-cell basis: (i) the preferred direction of stimulus motion, (ii) the mean percent change in firing rate induced by upward stimulus motion, and (iii) patterns of temporal firing probability. These results suggest that CS may contribute to long-term interactions between parallel and climbing fiber inputs, such as long-term depression and/or potentiation.

Chapter 2

INTRODUCTION

2.1 Internal model of controlled object

Despite controlled object can be described as multi-variable and nonlinear systems, biological movement are well-organized. These movements may be achieved by internal model of controlled object in the brain. Theoretically, internal models of the motor system were divided into two types: forward model and inverse model (Figure 2.1). An inverse model is a model system whose input and output correspond to the output and input, respectively, of the controlled object. It makes an ideal feed-forward controller and can be used for trajectory planning (Kawato and Gomi 1992a).

2.2 Inverse model and cerebellum

The existence of the internal model for motor control had already predicted by M. Ito (Ito 1970) over 20 years ago. Many behavioral and lesion studies have been suggested that the cerebellum may be a candidate for composing internal model. A remarkable feature of the Purkinje cells in the cerebellum is that each cell receives two major afferents that differ dramatically in their firing dynamics: a) multiple parallel fiber inputs that generate simple spikes (SS) at rates up to several hundred discharges per second and b) a single climbing fiber input that generates complex spikes (CS) at rates that do not exceed

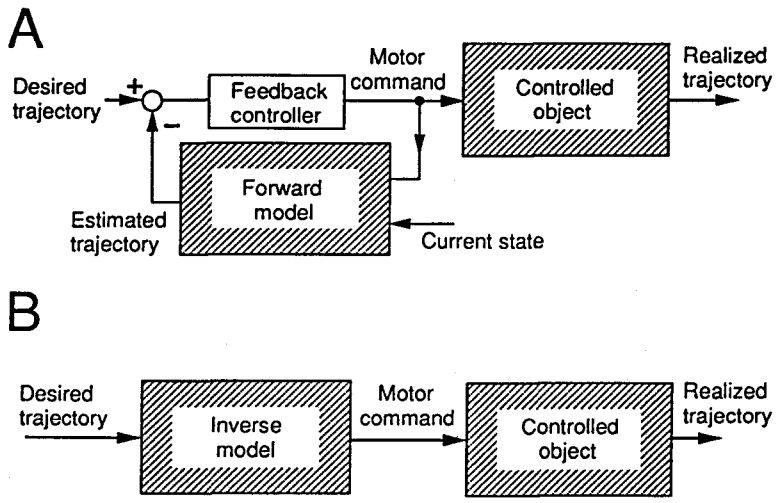

Figure 2.1: Feed-forward control using by forward (A) and inverse (B) model. (From Kawato and Gomi 1992a)

more than a few discharges per second (Thach 1968). Our group have shown physiological evidences about inverse model in the cerebellum. Recent modeling studies of temporal profiles of firing rate of SS of Purkinje cells in the cerebellum during ocular following responses using an inverse-dynamics model (a linear combination of eye acceleration, velocity, and position) demonstrated that SS in the VPFL encode dynamic motor commands (Shidara et al. 1993; Kawano et al. 1996; Gomi et al. 1997). These studies were based on the assumptions that if the inverse-dynamics model was constructed in the cerebellar cortex, the activity of the Purkinje cells (which are only output neurons in the cerebellar cortex) should encode torque for drive movement. During eye movement, three pairs of extra ocular muscles rotate eyes, and mechanical property of eye can be greatly simplified by 2nd-order dynamical system, so torque for moving eye can be represented by linear summation of inertia, viscocity and elasticity components. Consequently, the activity of the Purkinje cells should be represented by inverse-dynamics model (linear model of eye acceleration, velocity and position).

Figure2.2 shows the averaged SS, eye acceleration, velocity, position stimulus velocity. The figure shows eye movement occurred after 50 ms after the onset of the stimulus motion. Before the stimulus motion the firing rate of

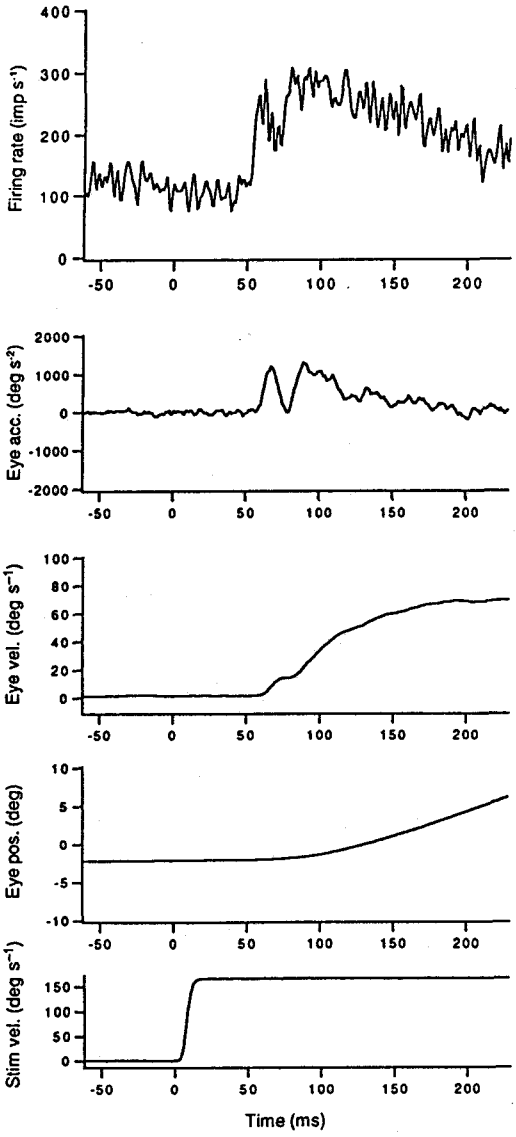

Figure 2.2: Temporal profile of SS firing rate during OFR Firing rate of SS, eye acceleration, velocity, position stimulus velocity were shown. Trial number was 65. (From Shidara et al. 1993)

the SS was constant at about 100 spikes/s. The firing rate was modulated synchronously with eye movement. The temporal patterns of eye movement was complex. That of the SS also complex. However, the complex temporal patterns of SS was well-predicted by linear summation of eye accerelation, velocity and position, that is the simplest model of second order dynamical system. The temporal pattern of the SS were reconstructed by following equations.

$$f(t) = M \cdot \ddot{\theta}(t+\delta) + B \cdot \dot{\theta}(t+\delta) + K \cdot \theta(t+\delta) + C \qquad (2.1)$$

$f(t)$ means firing rate in time t. $\ddot{\theta}$, $\dot{\theta}$, θ means acceleration, velocity and position of eye movement. δ means time-lag between firing and eye movement. M, B and K were estimated coefficient parameters in accerelation, velocity and position. C means coefficient for constant component (spontaneous firing rate). The model parameters were estimated by the minimum squared error method.

The reconstructed firing rate are shown in Figure 2.3. The difference between actual and modeled firing data were quite similar. The goodness of the model fit was statistically significant. Furthermore, the generality of the model was also confirmed by examining various pattern of movement and various firing patterns using several kinds of stimulus (Figure 2.3).

2.3 Visuo-motor signal transformation in the cerebellum

In previous studies (Kawano et al. 1992,1994, Shidara and Kawano 1993), neural substrates shown in Figure2.4 were involved in the generation of OFR. The firing rates of the MST and DLPN neurons, which provide visual inputs to the cerebellar cortex, are not well reproduced by the inverse dynamics model from the eye movement in response to a wide range of stimulus velocities (Kawano et al. 1994b). This supports the widely accepted idea that these two regions convey primarily visual information. This indicates that visuo-motor

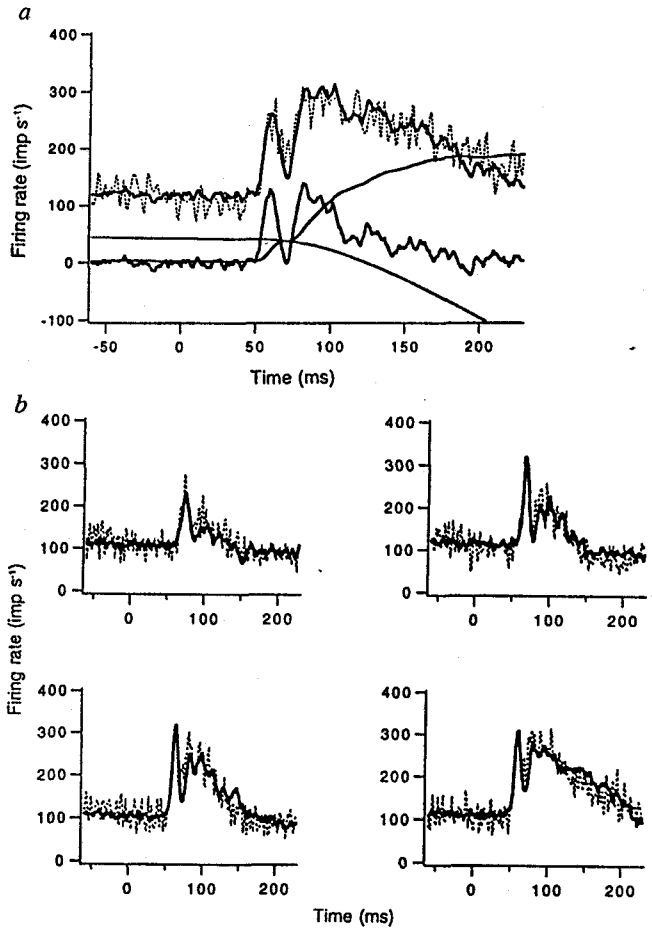

Figure 2.3: Reconstruction of SS by inverse-dynamics model (From Shidara et al. 1993). Dotted line showed raw data and Thick line showed reconstructed firing rate.

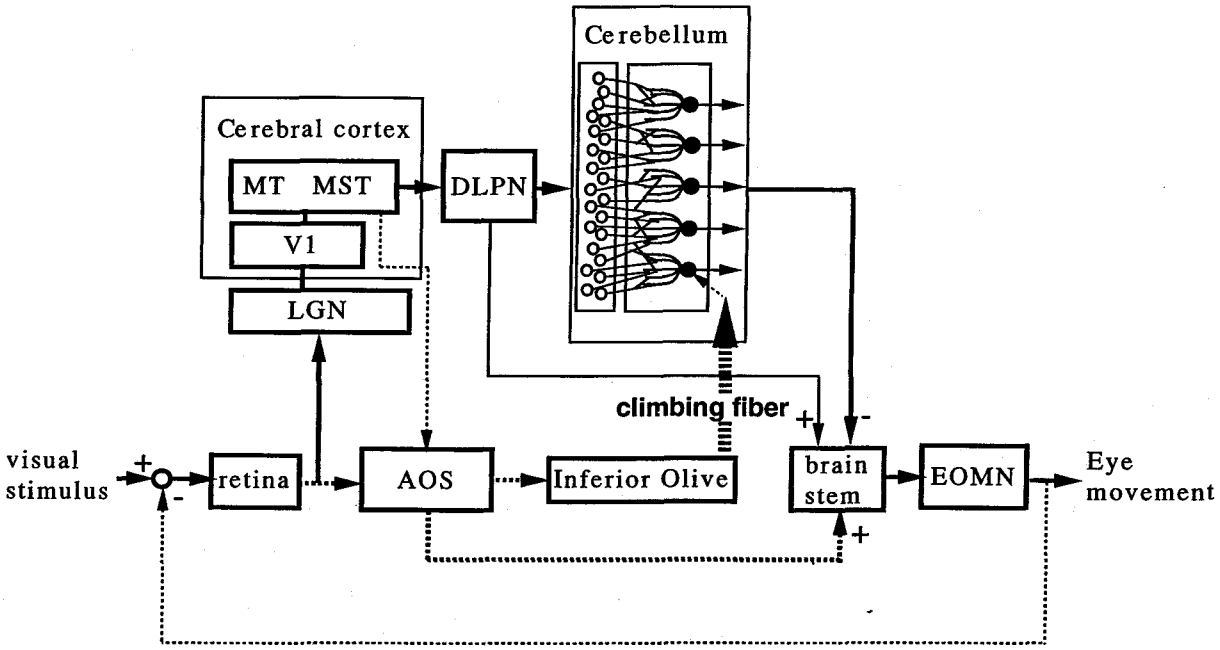

Figure 2.4: Neural substrates related to OFR (From Gomi et al. 1995)

signal transformation occurs in the cerebellum, and support the hypothesis the cerebellum executes computation of inverse-dynamics.

2.4 Analysis of firing probability using generalized linear model

In previous modeling studies (Shidara et al. 1993, Gomi et al. 1995) , the temporal patterns of instantaneous firing rate of the SS was modeled by linear summation of the eye acceleration, velocity and position. The model parameters were determined by the minimum squared error method. Although the firing rate is the values from 0 to 1, the firing rate was regarded as real value without constrains in that model. The model may be reasonable only the case that (1) firing rate is away from 0 or 1.0 and (2) the variance of estimated error obeys normal distribution. Thus it is difficult to analyze the temporal

pattern of CS because of its low firing rate. The present study proposes the new statistical method of utilizing for either low firing rate or small number of the accumulated trials. The method is based on the assumptions that in trail number m, the total number of the spike counts Y for individual time bin t obeys binomial distribution whose probability π. π was represented by the function composed with linear summation for some time-dependent functions operated sigmoid function, sigmoid function constrains probability π 0 to 1. The estimated parameters were calculated by maximum likelihood method using Fischer's Scoring method. Theoretically, the method can easily make the likelihood value to maximum. We can estimate degree of the fit and degree of the freedom of the model parameters by likelihood ratio (deviance) and can estimate confidence intervals of model parameters (Kawato 1995).

2.5 Hypotheses about function of complex spike

The type of information transmitted by the ultra-low CS firing rate and the effect of a signal with low temporal resolution on the cerebellum is still not completely resolved. The primary theories regarding the function of CS are summarized as follows.

Hypothesis (1): the unexpected event detector hypothesis

CS have been shown to be elicited by unexpected perturbations during wrist movements in awake monkeys (Gilbert and Thach 1977), during skilled locomotion (Andersson and Armstrong 1987) and a step-like movement (Gellman et al. 1985) in awake cats and during walking in decerebrate ferrets (Lou and Bloedel 1986, 1992).

Hypothesis (2): the error hypothesis

The word "unexpected" is not suitable because we can only guess what animals expects. Since the cerebellum is involved in controlling both posture and

movement, we have to argue whether a mismatch occurs between the desired and actual movement. In that sense, the unexpected sensory events should be considered as errors (Oscarsson 1980) in postural performance and movement. It has been suggested that the mean firing rate of CS over several hundred milliseconds represents a sensory error signal (e.g., retinal slip). This hypothesis was derived from experimental data obtained in the rabbit flocculus during eye movements induced by movement of a large visual field (Simpson and Alley 1974; Graf et al. 1988). Furthermore, in the monkey ventral paraflocculus (VPFL) during smooth pursuit eye movement induced by small target motion, transient retinal slip was shown to correlate with the occurrence of a single CS during steady-state pursuit (Stone and Lisberger 1990b). In Ojakangas and Ebner's study, CS was shown to be coupled to a velocity-related error signal during a voluntary arm movement (Ojakangas and Ebner 1994).

Hypothesis (3): the motor command hypothesis

The CS have been suggested to be real-time motor commands that modulate SS (Mano et al. 1986) because for tens of milliseconds after a CS, there is a pause in SS firing (Bell and Grimm 1969) and/or there is a short-term modulation of SS discharges for several hundred milliseconds after CS firing (Ebner and Bloedel 1981).

Hypothesis (4): the timing and synchronization hypothesis

The electrical coupling between inferior olive (IO) neurons (Llinás et al. 1974; Sotelo et al. 1974) has been shown to cause a degree of CS synchrony among groups of Purkinje cells (Sugihara et al. 1993; Wylie et al. 1995). In the vestibulocerebellum in alert rabbit CS synchrony was demonstrated during eye movement (De Zeeuw et al. 1997a). This characteristic, and the observation that CS have relatively rhythmic firing patterns (Welsh et al. 1995), has led to the suggestion that CS are phasic motor commands involved in controlling

the timing of movement execution.

Hypothesis (5): the learning hypothesis

Results of physiological, anatomical, and behavioral studies, as well as the existence of long-term depression at parallel-fiber/Purkinje-cell synapses, support the proposal that the climbing fibers are involved in motor learning. In summary, SS provide motor commands that are regulated by CS via modulation of the efficacy of the parallel fiber inputs (Marr 1969; Albus 1971; Ito 1984).

Kawato and colleagues extended earlier learning models by formulating a computationally explicit feedback-error-learning model. In this model, CS are assumed to be copies of feedback motor commands generated by a crude feedback control circuit, and, thus CS are suggested to be sensory error signals in motor coordinates. The model predicts that the cerebellar cortex acquires an inverse dynamics model of a controlled object as a result of this learning (Kawato et al. 1987; Kawato and Gomi 1992a,b). There is an ongoing debate as to whether the plasticity at the parallel-fiber/Purkinje-cell synapse is the elementary process underlying motor adaptation and motor learning and what role climbing fibers may have in this process.

These hypotheses variously predict the information conveyed by CS, the relationship between SS and CS, and the function of CS. The information conveyed by CS is suggested to be either the occurrence of an unexpected event (hypothesis 1), sensory error (hypotheses 2 and 5), motor commands (hypothesis 3), or timing of movement (hypothesis 4). The feedback-error-learning model (Kawato and Gomi 1992b) predicts intermediate properties of CS, that is, that CS are derived from sensory error signals but are already represented temporally and spatially as feedback motor commands. CS and SS are suggested to be either independent (hypotheses 1, 2, and 4) or related via short-term modulation (hypothesis 3) or long-term synaptic plasticity (hypothesis 5). The function of CS is suggested to involve either real-time motor control (hypotheses 2, 3, and 4) or motor learning (hypothesis 5). However

these hypotheses are not necessarily mutually exclusive. Dual function is also possible.

The present study quantitatively examines CS function by examining CS and SS responses in the VPFL during ocular following responses (OFR) in awake monkeys (Miles et al. 1986) and quantifying the relation between the two discharges and retinal slip and eye movement. Recent modeling studies of SS temporal firing profiles during OFR using an inverse-dynamics model (a linear combination of eye acceleration, velocity, and position) demonstrated that SS in the VPFL encode dynamic motor commands (Shidara et al. 1993; Kawano et al. 1996; Gomi et al. 1997). In the present study, in addition to the electrophysiological experiments, this model was extended to a more sophisticated generalized linear model (Kawato 1995) to analyze the correlation between the ultra-low CS firing rate and the motor commands or retinal slip.

2.6 The VPFL and Ocular Following Responses

OFR are tracking movements of the eyes evoked by movements of a visual scene and are thought to be important for the visual stabilization of gaze. It was advantageous to study CS function by recording them in the VPFL during OFR for several reasons.

The OFR are primarily under negative feedback control, because this behavior is primarily in response to retinal slip, which is the difference between the image motion and the eye movement. The early phase of the OFR, however, is controlled in an open-loop manner, and this early phase has been shown to be subject to long-term adaptive modification by visual error signals (Miles and Kawano, 1986). OFR are reflexes induced by the retinal slip, thus, it is technically easy to obtain a large number of trials, thus increasing the signal-to-noise ratio. It is possible to quantify the correlation between the sensory error signal (retinal slip) and CS firing, because it is possible to accurately control the parameters of the visual stimulus.

The latency of OFR after the stimulus motion is about 50 ms, which is very

short compared with a latency of 80 ms for the smooth pursuit eye movement (Lisberger and Westbrook 1985). The short latency and the reflex nature of OFR suggest that the neural circuitry underlying OFR are relatively simple.

The VPFL has been implicated in the genesis of the earliest components of the OFR. This is suggested by studies demonstrating that a single, low current electrical stimulation of the VPFL induces downward or ipsilateral eye movement (Shidara and Kawano 1993) and lesions of the VPFL abolish a large portion of the OFR (unpublished observation referred in Miles et al. 1986). The medial superior temporal area of cerebral cortex (MST) and the dorsolateral pontine nucleus (DLPN) provide visual information to the VPFL during OFR (Kawano et al. 1992, 1994a, b), and this pathway (MST-DLPN-VPFL) has been suggested to be a major sensory-motor transformation circuit (Glickstein et al. 1985; Langer et al. 1985; Tusa and Ungerleider 1988; Kawano et al. 1992, 1994a, b).

Most MST and DLPN neurons showed strong directional preferences for visual stimulus motion, and when their preferred directions (directions of movement associated with the most vigorous discharges) are plotted together in polar form it is clear that all directions of motion are represented about equally (Kawano et al 1992, 1994a).

The preferred direction of SS and CS, and their reference frame was extensively examined in the rabbit during OKR, using 3-D planetarium projector (Graf et al. 1988). The coordinate systems of eye muscles and semicircular canals are similar in both frontal and lateral eyed animals (Graf and Simpson 1981). The reference frames of SS and CS were found aligned with those of extraocular muscles or semicircular canals (Graf et al. 1988). The axes of the reference frame of frontal-eyed animal shown to be approximately horizontal and vertical in front-parallel plane (Simpson et al. 1986). The preferred directions of SS and CS recorded in the VPFL has also been previously characterized during the smooth-pursuit eye movements involved in tracking a small target (Stone and Lisberger 1990a, b; Krauzlis and Lisberger 1996). They concluded that the preferred directions of SS in the VPFL were either downward

or ipsilateral in front-parallel plane, and were aligned in the reference frame of either semicircular canals or extraocular muscles (Krauzlis and Lisberger 1996).

SS evoked during OFR have been recorded and characterized in Purkinje cells in the VPFL (Shidara and Kawano 1993; Shidara et al. 1993, Kawano et al. 1996). The preferred directions of SS during OFR were also either downward or ipsilateral (Shidara and Kawano 1993; Shidara et al. 1993, Kawano et al. 1996).

2.7 Complex spikes in the VPFL

The projections from the inferior olive to the climbing fibers in the VPFL have been well characterized (Gerrits and Voogd 1982, 1989; Langer et al. 1985). In the rabbit flocculus, a large number of CS are evoked by movement of a large visual stimulus (Simpson and Alley 1974; Graf et al. 1988). CS were also recorded in the VPFL of monkeys during tracking of a small target (Stone and Lisberger 1990b). Thus, a considerable number of CS are expected to be evoked in the VPFL during OFR.

The CS in the VPFL have been previously well characterized during smooth pursuit eye movement (Stone and Lisberger 1990b). They concluded that CS were driven by the contralaterally or upward directed image motion. CS were modulated out-of-phase with SS. By spike-triggered averaging analysis, they concluded that CS during steady-state pursuit were shown to be driven by the retinal slip associated with imperfect pursuit.

2.8 Purpose of the present study

In this study, we advanced quantitative understandings of CS during OFR in the following four points, and have provided critical data to examine the major theories of CS functions. First, we developed a new statistical method for quantitatively analyzing what information was encoded in the temporal patterns of firing rate of CS. With this new technique, we demonstrated that

the CS firing probability carries very high frequency temporal information which matches that of the SS. Second, cell-to-cell negative correlations between the firing characteristics of SS and CS for individual cells were revealed. Third, although in previous studies the sensory aspects of CS were well studied, the new evidence for motoric nature of CS was added. Fourth, we examined the relationship between velocity amplitudes of eye movement or retinal slip and firing rates of CS over a wide range of data in response to various amplitudes of the step ramp speed.

Chapter 3

METHODS

3.1 Surgery

Data were collected from four adolescent monkeys (*Macaca fuscata*) that had been previously trained to fixate on a small spot to obtain a fluid reward. Each monkey was anesthetized with sodium pentobarbital and, in aseptic conditions, were implanted with a cylinder for microelectrode recording, a head holder that allowed the head to be positioned in a standard stereotaxic position during the experiments, and scleral search coils for measuring eye movements (Judge et al. 1980). All experimental protocols were approved by the Electrotechnical Laboratory Animal Care and Use Committee.

3.2 Behavioral paradigm

The behavioral paradigms and visual stimuli used to elicit OFR have been described previously (Kawano et al. 1992). The animals faced a translucent tangent screen (85 deg × 85 deg at a distance of 235 mm) on which moving Julesz random-dot patterns (Julesz 1971) were back-projected (Figure 3.1). The visual stimulus started to move 150 ms after the end of a centering saccade. Each visual stimulus ramp lasted 250-300 ms.

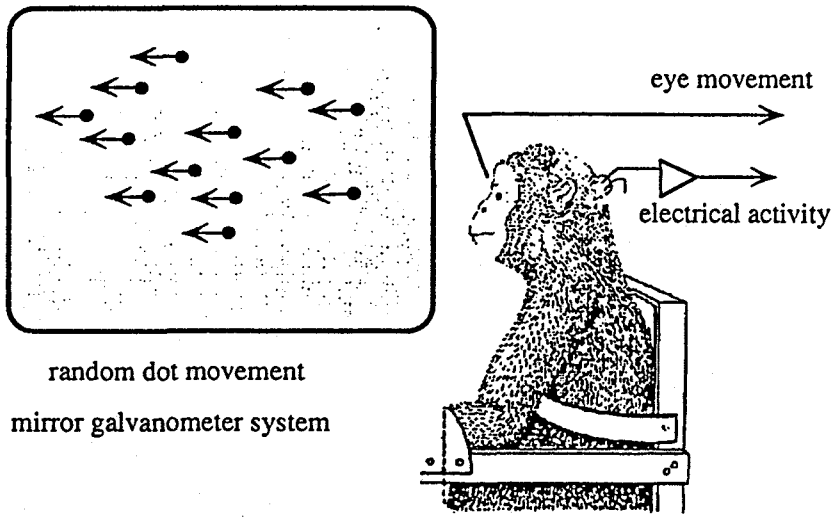

Figure 3.1: Experimental set up

3.3 Visual stimuli

Visual stimuli were designed to study the directional selectivity of neural firings (Experiment 1), effects of changes in stimulus velocity on neural firings (Experiment 2), and temporal patterns of firing rate and firing probability (Experiment 3).

Experiment 1

The directional firing characteristics of 13 cells were examined by moving the stimuli in eight directions (θ = 0, 45, 90, 135, 180, 225, 270, 315 deg) at a constant speed of 80 deg/s (Figure 3.2). The stimulus was presented and moved at least 40 times (40-77 trials, mean = 57 trials) in each direction while recording from each cell (320-616 trials, mean = 456 trials altogether). Because the latency of the change in SS firing rate during the OFR is about 40 ms from the onset of stimulus motion (Shidara and Kawano 1993), the

spike modulation for each stimulus direction was calculated as the mean firing rate over an interval extending from 40 to 220 ms after the onset of stimulus motion subtracted by the spontaneous firing rate, which was calculated as the mean firing rate over an interval from -100 to 40 ms after the onset of stimulus motion. The preferred direction of SS or CS of each cell was calculated as the direction of the average vector of the following eight modulation vectors. The modulation vector for each direction was defined as a two-dimensional vector with the same direction as the stimulus motion (θ) and a length equal to the spike modulation defined above. Since we did not use the 3-D planetarium projector system (Graf et al. 1988), we can not directly argue about the preferred axis of rotation in the 3-D space from our experimental data.

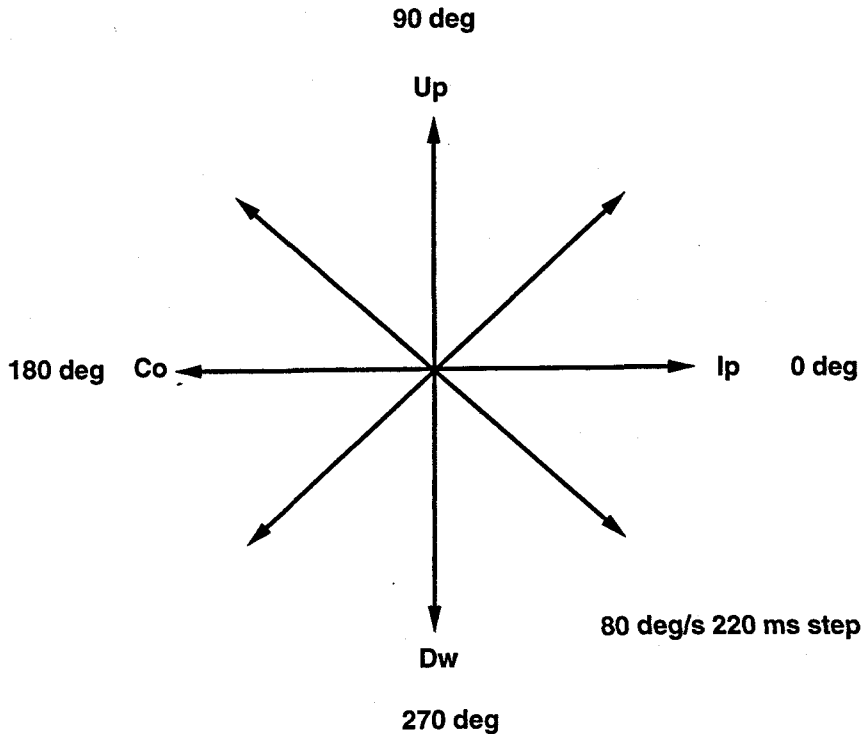

Figure 3.2: Behavioral paradigm for directional selectivity

Experiment 2

Stimuli moving at six or eight different velocities (+80, +40, +20, -20, -40, and -80 deg/s or +80, +40, +20, +10, -10, -20, -40, and -80 deg/s) were presented while recording from 12 cells (Figure 3.3). For each cell, the stimulus was moved either vertically or horizontally, so that it would overlap with the preferred and anti-preferred directions of SS. Upward and contralateral motion was assigned positive polarity. At least 70 trials (76-217 trials, mean = 134 trials) were performed at each stimulus velocity for each cell (608-1592 trials, mean = 948 trials).

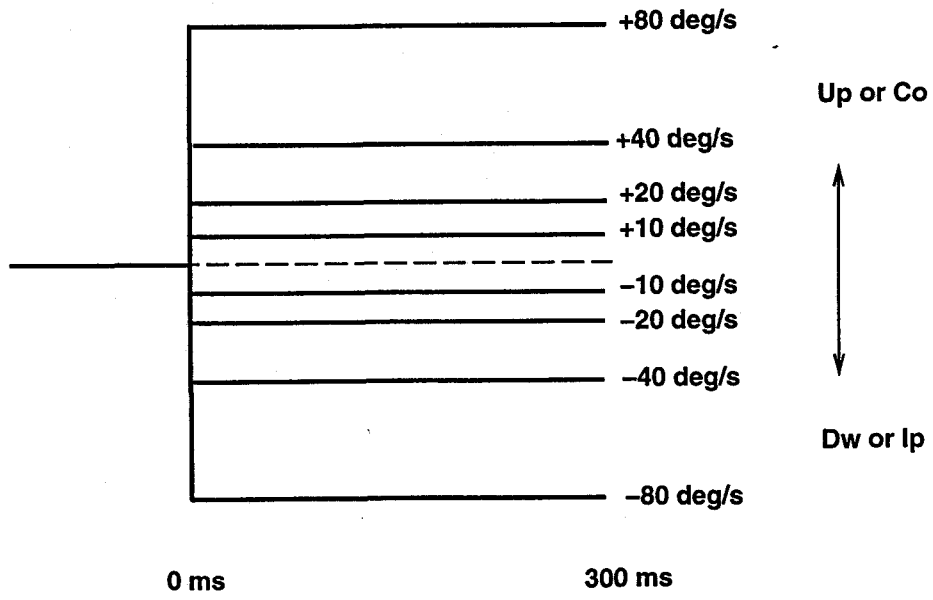

Figure 3.3: Behavioral paradigm for speed tuning

Experiment 3

Stimuli moving directly upward at 80 deg/s were presented to nine vertical axis cells (V cells). For V cells, directly upward is close to the preferred direction of CS and the anti-preferred direction of SS. Upward moving stimuli were presented more than 300 times (312-901 trials, mean = 579 trials) while recording from each cell.

For improving data reliability in the analysis of firing characteristic of CS for each cell, we focused on obtaining a large number of trials rather than to increase a number of recorded cells.

3.4 Recording technique

At the beginning of each recording session, a monkey was moved from its home cage to a custom-made acrylic chair, where its head was fixed to the chair frame via the implanted head holder. A hydraulic microdrive (Narishige Mo-9) was mounted on the recording cylinder, and glass-coated tungsten microelectrodes were used for the initial identification of the VPFL. In some cases, after locating the VPFL, a stainless steel guide tube was introduced through the dura matter and the tentrium and held in place by cementing it to the side of the recording cylinder while the animal was sedated with ketamine hydrochloride. Flexible tungsten electrodes lowered into the brain through the guide tube were used to record cellular activity.

The methods of collection, storage, and display of the neural and ocular responses were similar to those described previously (Kawano et al. 1992). A DAT recorder (SONY PC208A) was used to store analog data. An electromagnetic induction technique was used to monitor eye movements. The DC voltage outputs proportional to horizontal and vertical eye position were low-pass filtered with 6-pole Bessel filters (cut-off; 100 Hz). Eye-position measurements were subjected to analog differentiation to provide outputs proportional to eye velocity with a bandpass of DC-500 Hz (-3 dB). Voltage signals separately encoding the horizontal and vertical components of eye position, eye velocity, and mirror (stimulus) velocity were digitized at a resolution of 16 bits, sampling at 1 kHz.

Purkinje cells were identified by the presence of SS and CS (Thach 1968). Before trial sessions, we carefully discriminated single unit by time-amplitude window discriminator and we checked CS and SS were derived from a single cell by confirming the brief pause of the SS by CS (Sato et al. 1992). After the

sessions, SS and CS were discriminated with a time resolution of 1 or 2 ms off-line using the custom software which clusters groups of spikes by amplitude, duration and wave form by the principal component analysis running on a SUN SPARK station.

3.5 Generalized linear model

Difficulty in parameter estimation for temporal profile of CS firing rate

In previous studies, the SS firing rate was directly reproduced using an inverse-dynamics representation model, which is a linear weighted summation of the eye acceleration, velocity, and position (Shidara et al. 1993; Kawano et al. 1996; Gomi et al. 1997). The very low CS firing rate precludes the direct use of this method for the analysis of the CS temporal firing profile, however, the firing probability rather than the firing rate itself can be modeled. The low CS firing rate highlighted the binomial nature of the spike count. The variance was not constant, invalidating the minimum-square-error method for parameter estimation, and the standard deviation had the same magnitude as the mean, rendering the correlation coefficient rather insensitive to the goodness-of-fit.

Sampling noise in the CS

The fluctuations in the CS firing rate were largely due to the variance of the binomial distribution (Figure 3.4). Theoretically, the firing rate (spikes/s) multiplied by the time bin (s) converges to the firing probability p as the trial number n goes to infinity with a standard deviation $\sqrt{p(1-p)/n}$ of the binomial distribution. The following is a typical example of a firing probability with the same order of magnitude as its standard deviation. The standard deviation 0.003 is close to the signal itself for $p = 0.005$ (2.5 spikes/s multiplied by a 2-ms bin) and $n = 500$. Thus, for CS, the low value of the actual correlation coefficient and the predicted value does not necessarily mean a

poor fit by the model. On the other hand, for SS, firing at 100 spikes per second, the signal (i.e., probability $p = 0.2$) is much larger than the noise (i.e., the standard deviation is 0.02) and thus, use of the correlation coefficient is valid.

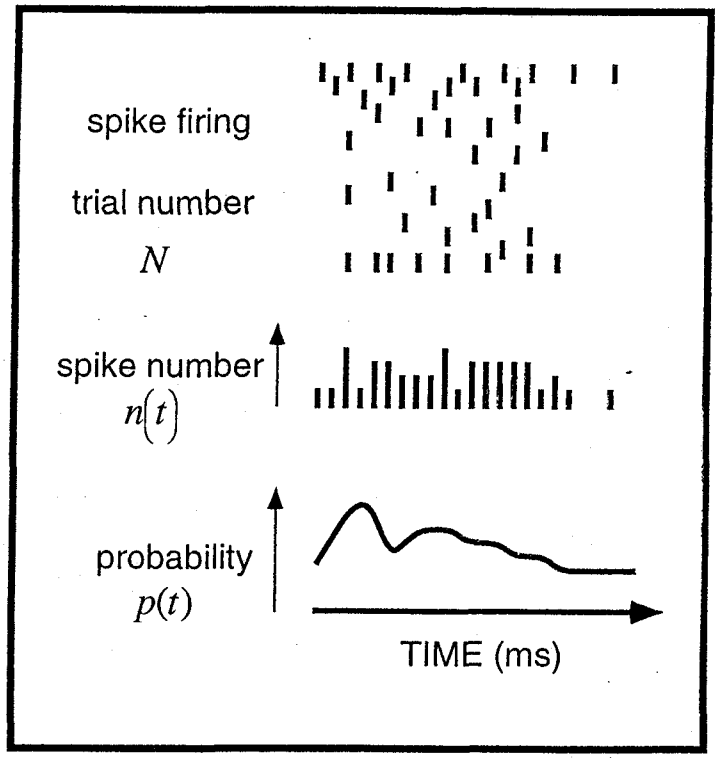

Figure 3.4: Schema indicating the binomial distribution of spike counts

Application of generalized linear model of eye movement for firing probability

We confirmed that the number of CS, X_i, that accumulated within the time $t = i$ bin for n trials, obeyed the following binomial distribution (Kobayashi et al. 1995).

$$\Pr\{X_i = y_i\} = \begin{pmatrix} n \\ y_i \end{pmatrix} p_i^{y_i}(1 - p_i)^{n-y_i} \tag{3.1}$$

where y_i denotes the realized value of the stochastic variable X_i, that is, the observed spike number. p_i is the spike occurrence probability within the time

$t = i$ bin. The CS firing probability $p(t)$ as a function of time t was modeled by the following generalized linear summation of acceleration, velocity, and position of eye movement, which is a smooth function of time.

$$p(t) = S[M \cdot \ddot{\theta}(t+\delta) + B \cdot \dot{\theta}(t+\delta) + K \cdot \theta(t+\delta) + C] \tag{3.2}$$

$$S[x] = \frac{\exp x}{1 + \exp x} \tag{3.3}$$

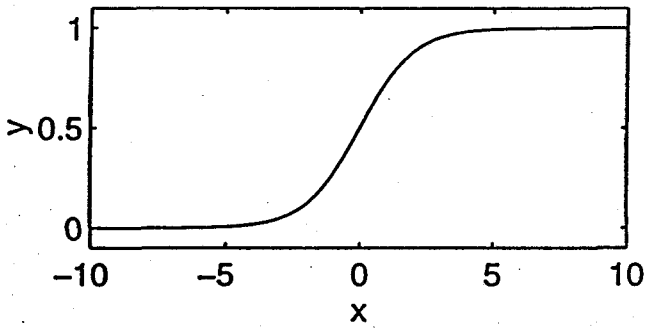

Figure 3.5: The sigmoid function S constrains $p(t)$ to values between 0 and 1.

where $\ddot{\theta}$, $\dot{\theta}$, and θ denote the acceleration, velocity, and position of the eye, and M, B, and K denote their coefficients, respectively, while δ denotes the time delay between CS discharge and eye movement, and C is a constant. The sigmoid function S constrains $p(t)$ to values between 0 and 1 (Figure 3.2). This is a specific example of a generalized linear model (McCullagh and Nelder 1989).

The parameters other than the time delay were estimated using Fisher's

scoring method by maximizing the following likelihood function, L or its logarithm l (the maximum likelihood method).

$$\begin{aligned} L(\boldsymbol{p};\boldsymbol{y}) &= \prod_{i=1}^{m} \Pr(X_i = y_i) \\ &= \prod_{i=1}^{m} \begin{pmatrix} n \\ y_i \end{pmatrix} p_i^{y_i}(1-p_i)^{n-y_i} \\ l(\boldsymbol{p};\boldsymbol{y}) &= \sum_{i=1}^{m} \{y_i \log p_i + (n-y_i)\log(1-p_i)\} \end{aligned} \tag{3.4}$$

m is the bin number included in one experiment. In Experiment 3, m=126, because all of the spike counts within a 2 ms bin were collected to calculate y_i from 0 to 250 ms after the onset of stimulus motion. m=756 (six velocities) or m=1008 (eight velocities) in Experiment 2, because stimuli with different velocities produced different sets of data. The time delay leading to the maximum likelihood was globally searched at every 2 ms step from -20 to 20 ms from the onset of stimulus motion.

Let L_1 denote the likelihood evaluated by the maximum likelihood estimator in p_i ($\tilde{p}_i = y_i/n$), which is the best possible model but with a large degree of freedom m, while L_0 denotes the maximum likelihood of the current model. If the model is good, the likelihood ratio ($\lambda = L_0/L_1$) is close to 1, but if the model is poor, the ratio approaches 0. The deviance D, $-2\log\lambda$ expressed in the following equation is always positive and approaches zero as the fit becomes better and becomes large as the fit becomes poorer.

$$\begin{aligned} D(\boldsymbol{y};\hat{\boldsymbol{p}}) &= 2l(\tilde{\boldsymbol{p}};\boldsymbol{y}) - 2l(\hat{\boldsymbol{p}};\boldsymbol{y}) \\ &= 2\sum_{i=1}^{m} \{y_i \log \frac{y_i}{n\hat{p}_i} + (n-y_i)\log\frac{n-y_i}{n-n\hat{p}_i}\} \end{aligned} \tag{3.5}$$

Generally, a smaller deviance indicates a better fit. Because the deviance increases in proportion to m, the deviances in Experiment 2 were divided by 6 or 8 (the number of different stimulus velocities) for comparison with that of Experiment 3 in Table 4.2. The SS firing probability was analyzed using the same method.

Application of generalized linear model of retinal slip

To further examine the sensory and motor characteristics of CS and SS, we compared the ability of a model based on the sensory error and the eye movement to reproduce the firing probability. Thus, the model was based on a generalized linear combination of the acceleration, velocity, and the position of the retinal slip as well (the difference between stimulus position and eye position):

$$p(t) = S[M_r \cdot \ddot{r}(t-\Delta) + B_r \cdot \dot{r}(t-\Delta) + K_r \cdot r(t-\Delta) + C_r] \tag{3.6}$$

where $\ddot{r}$, $\dot{r}$, r, C_r, and Δ denote the acceleration, velocity, and position of the retinal slip, a constant, and the delay between the onset of stimulus motion and spike discharge, respectively. The delay between the retinal slip and the spikes was globally searched from 30 to 70 ms after the onset of stimulus motion.

Test of number of covariates in the model

The deviance function is most directly useful not as an absolute measure of goodness-of-fit but for comparing two nested models. Because the χ^2 approximation is usually quite accurate for differences of deviances even though it is inaccurate for the deviance themselves.

$$\begin{aligned} D(\boldsymbol{y};\hat{\boldsymbol{\pi}}_0) - D(\boldsymbol{y};\hat{\boldsymbol{\pi}}_A) &= 2l(\hat{\boldsymbol{\pi}}_A;\boldsymbol{y}) - 2l(\hat{\boldsymbol{\pi}}_0;\boldsymbol{y}) \\ &= 2\sum_{i=1}^{n}\{y_i \log\frac{\hat{\pi}_i^A}{\hat{\pi}_i^0} + (m-y_i)\log\frac{1-\hat{\pi}_i^A}{1-\hat{\pi}_i^0}\} \end{aligned} \tag{3.7}$$

For instance, we may wish to test whether the addition of a further covariate significantly improves the fit. Let H_0 denote the model under test H_A the extended model containing an additional covariate. The corresponding fitted values are denoted by $\hat{\pi}_i^0$ and $\hat{\pi}_i^A$ in time i. The reduction in deviance is identical to the likelihood-ratio statistic for testing H_0 against H_A. When the difference of freedom between two nested model is q, χ^2 approximation which freedom is q is used.

Histology

At the conclusion of the experiments, the monkeys were deeply anesthetized with Nembutal and perfused intracardially with saline followed by 10% formalin. The brain was removed, frozen, cut into 50 μm parasagittal sections, mounted on microscope slides, and stained for histological study. Recording sites were marked by placing electrolytic lesions at select recording sites and verified to be in the VPFL by histological reconstruction of the electrode tracks.

Chapter 4

RESULTS

4.1 Electrical activity of Purkinje cell in the VPFL

Figure 4.1 shows upward 80 deg/s stimulus motion (A), eye velocity (B) and electrical activity of Purkinje cell in the VPFL. Negative and mono-phasic spikes were categorized simple spikes and multi-phasic spikes were categorized complex spikes (Eccles et al. 1966, Thach 1968).

CS and SS during OFR

We recorded SS and CS during OFR from 34 Purkinje cells. Figure 4.2 shows stimulus and eye movement (velocity, acceleration, and position), and examples of the responses to upward and downward stimulus motion at 80 deg/s. The characteristic short latency (about 50 ms from stimulus to movement) and the complex acceleration of OFR were evident (Miles et al. 1986).

The Purkinje cells were categorized into two groups. One population (23/34 cells) exhibited an increase in CS and a decrease in SS firing rate in response to upward moving stimuli (Figure 1G), and an increase in SS and a decrease in CS firing rate in response to downward moving stimuli (Figure 1H). These cells were termed V cells. The other population (11/34 cells) exhibited an increase in SS and a decrease in CS firing rate in response to ipsilateral stimulus

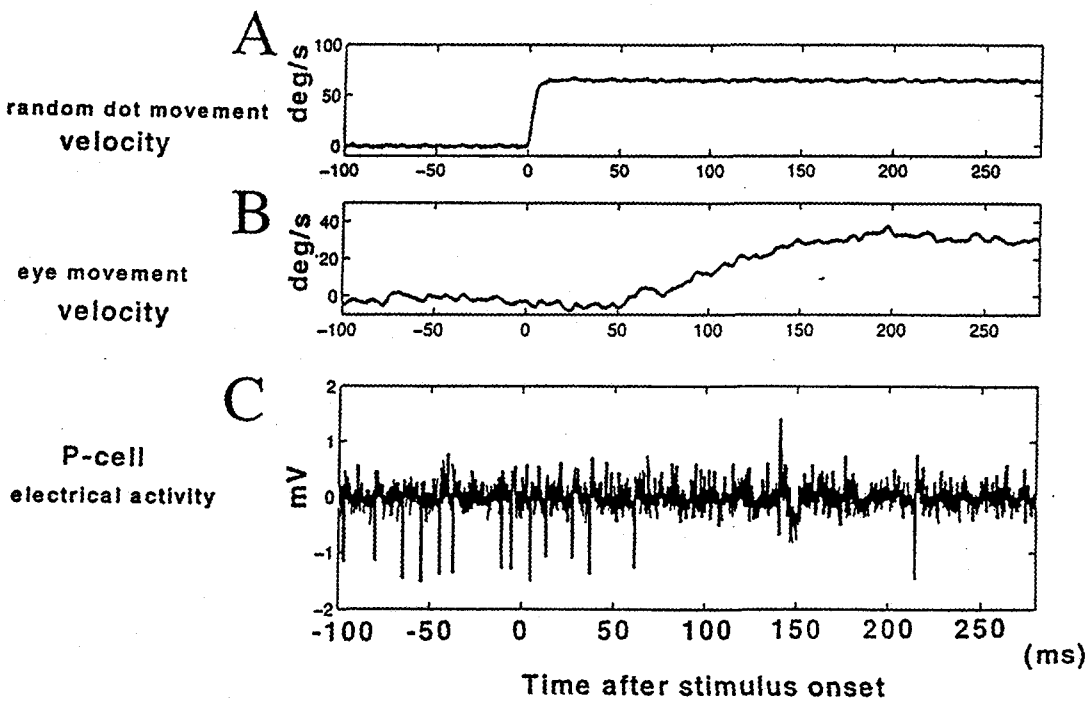

Figure 4.1: Electrical activity of Purkinje cell in the VPFL (A)Upward 80 deg/s stimulus motion, (B)eye velocity, (C)SS (Negative) and CS (multi-phasic). 0ms means onset of the stimulus motion.

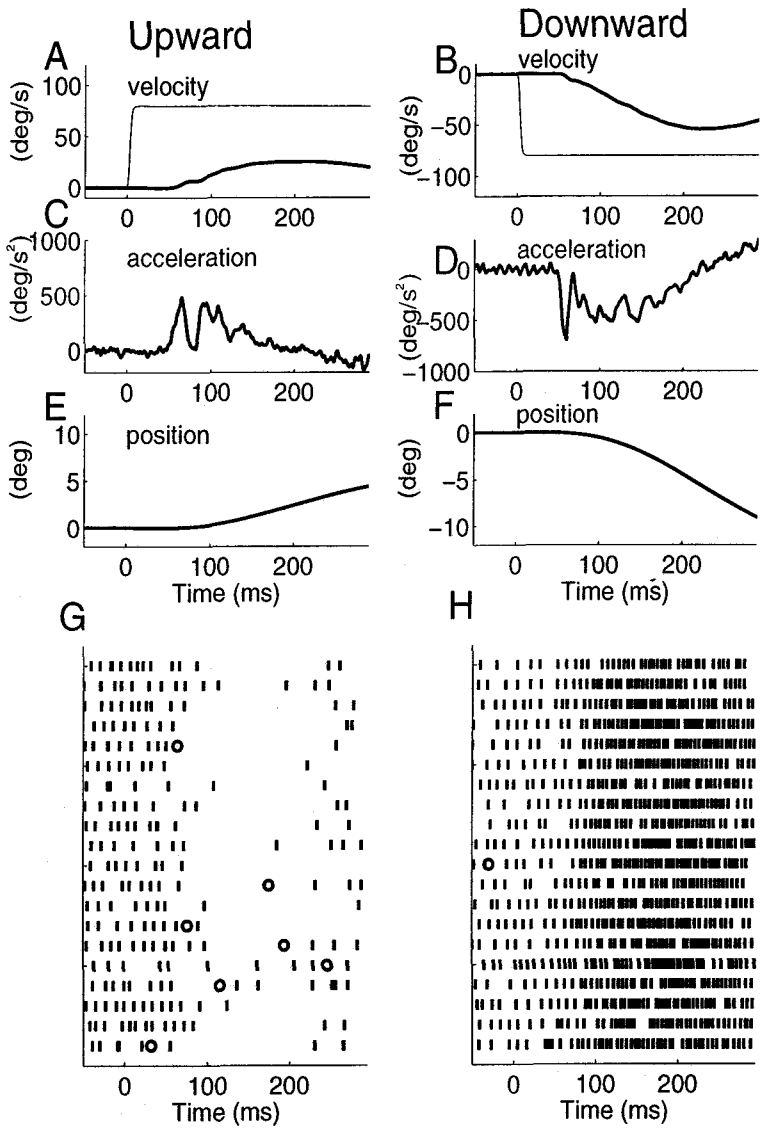

Figure 4.2: Eye movements and CS and SS during OFR. The left column shows responses to 80 deg/s upward stimulus motion, and the right column shows responses to 80 deg/s downward stimulus motion. Stimulus velocity (thin line in A and B) and eye velocity (thick line in A and B), eye acceleration (C and D), and eye position (E and F) as functions of time after the onset of stimulus motion during OFR are shown. G and H show examples of rastergrams of the SS and CS responses in a V cell during OFR to 20 presentations of upward (G) and downward (H) test ramps. The bars represent SS and the circles represent CS.

motion, and an increase in CS and a decrease in SS firing rate in response to contralateral stimulus motion. These cells were termed horizontal cells (H cells).

4.2 Directional tuning of CS

To quantify the spatial tuning characteristics of SS and CS, the responses to moving the stimulus in eight different directions at 80 deg/s were recorded (Figure 4.3). The aggregated activities of eight V cells are shown.

Both SS and CS were modulated by vertically moving stimuli, but they were not modulated by horizontal stimuli. Both SS and CS had some degree of spontaneous firing. Downward moving stimuli elicited increases in the SS firing rate approximately 40 ms and decreases in CS rate, both beginning after the onset of stimulus motion. Upward moving stimuli elicited decreases in the SS firing rate and increases in CS rate with similar (40 ms) latencies. The latencies of the changes in SS and CS are more quantitatively examined later by analysis of their temporal profiles.

The preferred directions of SS and CS for individual cells were shown in Figure 4.4A and B. Preferred directions of the SS and CS for each cell were calculated according to the method described in METHODS. The mean of the preferred directions of SS for V cells was 273.7 ± 27.4 (deg) (mean ± SD), that of SS for H cells was 1.8 ± 6.7 (deg) (mean ± SD), that of CS for V cells was 84.7 ± 10.7 (deg) (mean ± SD), CS for H cells was 189.4 ± 5.6 (deg) (mean ± SD). The mean difference between the preferred directions of SS and CS was 173 ± 16 (deg) (mean ± SD), which is close to 180 deg (Figure 4.4A and B). Thus, the reciprocity between the preferred direction of SS and CS was shown.

To quantify the directional dependency of the SS and CS modulations, the directional tuning data of SS or CS averaged over the V cell or the H cell population were fitted by a cosine function of the direction of stimulus motion:

$$f = a[\cos(\theta - \theta_p)] + b \tag{4.1}$$

where f and θ denote the mean firing rate and the direction of stimulus movement (θ = 0, 45, 90, 135, 180, 225, 270, 315 deg), respectively. The preferred directions of the averaged data (θ_p) were computed by averaging the preferred directions across the population. a and b denote the regression coefficient and the intercept of the regression equation, respectively which were

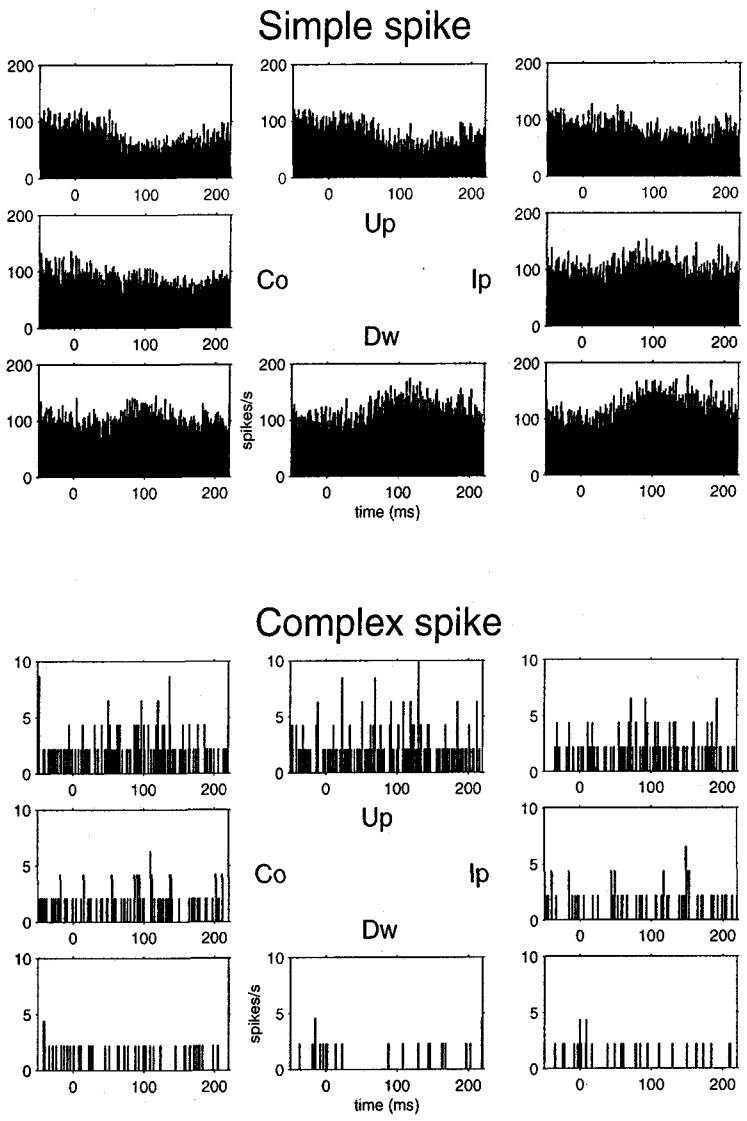

Figure 4.3: SS and CS peristimulus histograms in response to moving the stimulus in eight different directions. The aggregated responses from eight V cells are shown. The position of each histogram corresponds to the direction of the stimulus motion. (Ip: ipsilateral, Up: upward, Co: contralateral, Dw: downward)

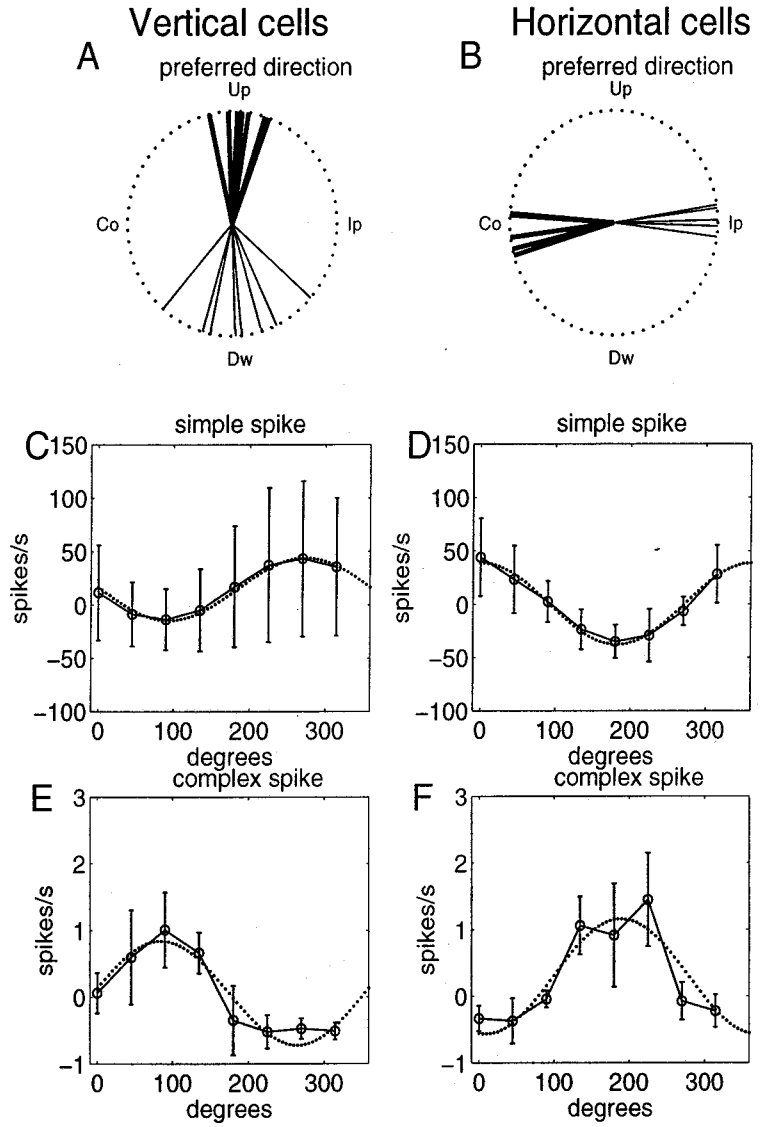

Figure 4.4: Directional tuning properties of SS and CS. The preferred directions of SS (thin lines) and CS (thick lines) for eight V cells (A) and five H cells (B) are shown. C-F show the mean (±SD) modulation of SS and CS in V cells (C,E) and H cells (D,F) as a function of the direction of stimulus motion. The abscissa (C,D,E,F) is the direction of stimulus motion in degrees measured counter-clockwise from the ipsilateral direction (ipsilateral = 0 deg, upward = 90 deg, contralateral = 180 deg, and downward = 270 deg). The means were fitted by a cosine tuning function (dotted line).

determined by the least-square method. a and b indicate the magnitude of direction-dependent modulation of the firing rate and the spontaneous firing rate, respectively. For the SS data, (a, b) were (29.2, 14.8) in V cells and (38.2, 0.7) in H cells. For the CS data, (a, b) were (0.78, 0.06) in V cells and (0.86, 0.3) in H cells. The averaged data and the fitted curves are shown in Figure 4.4C-F. The data and the fitted curves were well correlated (r (correlation coefficient) =0.99 for SS in V cells, r=0.99 for SS in H cells, r=0.96 for CS in V cells, and r=0.90 for CS in H cells) indicating that the CS and SS directional tuning characteristics were well modeled by the cosine function. The cosine directional tuning curves of SS and CS were 180 deg out of phase. Because the mean direction-dependent modulation of the CS firing rate (a=0.82) was 0.024 of that of SS (a=33.7), the mean change in the CS firing rate depending on stimulus directions was only 2.4 % of that of SS.

When the preferred direction of SS was plotted against that of CS as in Figure 4.5, the slope of the regression line was close to 1.0 (0.82) and its intercept was close to 180 deg (155 deg). These results provide quantitative evidence that the spatial tuning properties (including the preferred direction) of CS are opposite to those of SS. In 13 cells examined, the preferred direction of SS recorded from each cell correlated with the preferred direction of CS recorded from the same cell with a coefficient of 0.90 (P=0.001). The data were separated into two clusters (i.e. H and V cells). Although no significant correlation existed when each cluster of data was regressed separately, the above significant correlation for all the data at least indicates global reciprocity of the preferred directions of the SS and CS.

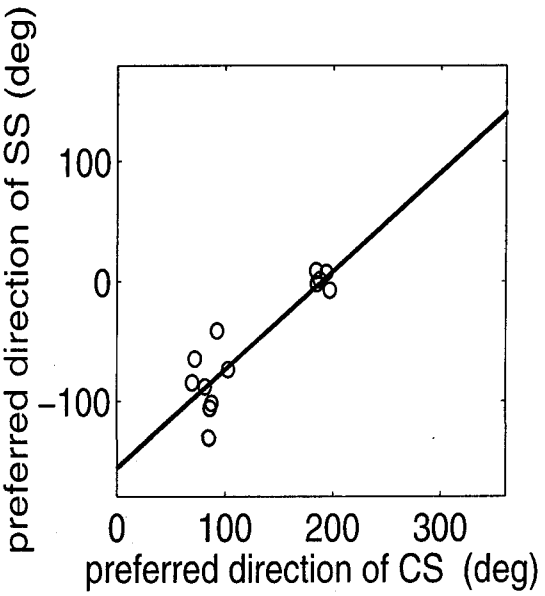

Figure 4.5: The preferred direction of SS for each cell is plotted against that of CS. The line represents the linear regression of the data.

4.3 Effects of stimulus velocity on CS and SS

Twelve cells were studied and findings for one example are shown Figure 4.6. The SS firing rate increased and the CS rate decreased with increased downward stimulus velocity (retinal slip velocity) and the resulting downward eye movement. Moreover, the SS firing rate decreased and the CS rate increased with increased upward stimulus velocity and the resulting upward eye movement.

To quantify the correlation between the SS and CS firing rates and retinal slip or eye velocities, the mean SS and CS firing rates were plotted against mean retinal slip and mean eye velocity. Considering its time delay, eye movement was averaged over the time interval from 50 ms to 300 ms after the onset of stimulus motion. SS and CS were averaged from 40 ms to 290 ms after the onset of stimulus motion. Retinal slip was averaged from 0 ms to 250 ms after the onset of stimulus motion.

The mean SS firing rate was a monotonically decreasing function of the slip velocity. The curve from each individual cell was a sigmoid function, that is, a decreasing, monotonic, saturating function (Figure 4.7A). In contrast, the

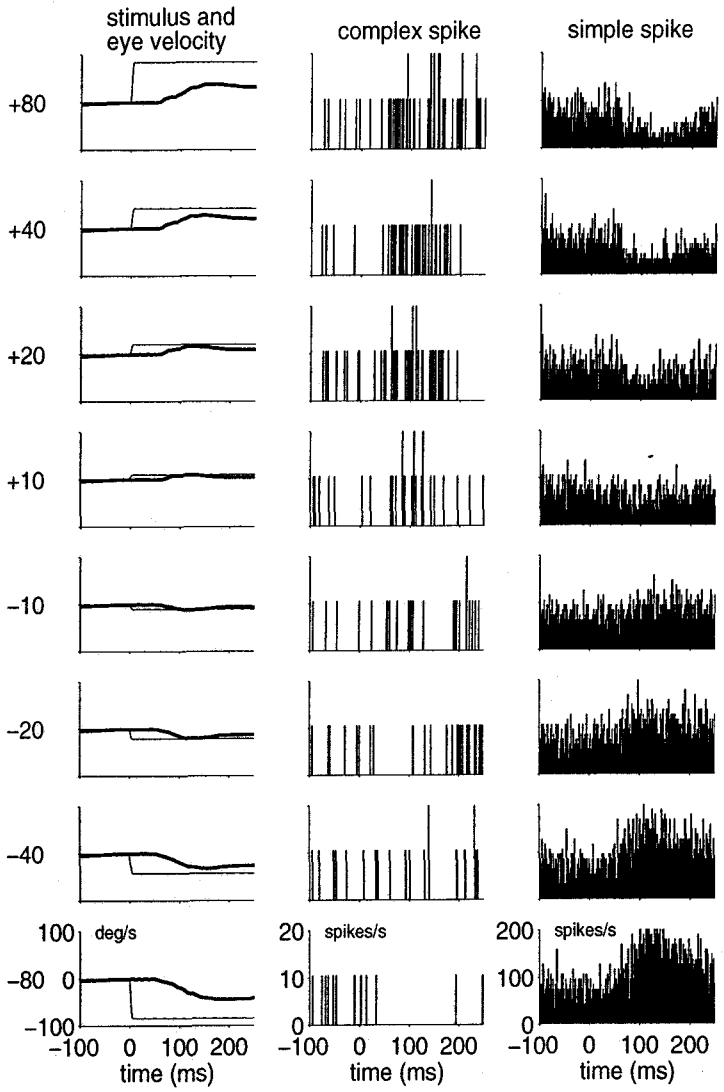

Figure 4.6: SS and CS of an example V cell in response to a wide range of stimulus velocities. The stimulus was moved vertically at +80, +40, +20, +10, -10, - -20, -40, and -80 deg/s. Upward motion was assigned positive polarity. Mean stimulus (thin line) and eye (thick line) velocities (left) and peristimulus time histograms with CS (middle) and SS (right) binned in 1 ms intervals are shown for each stimulus velocity for which 95 trials were obtained.

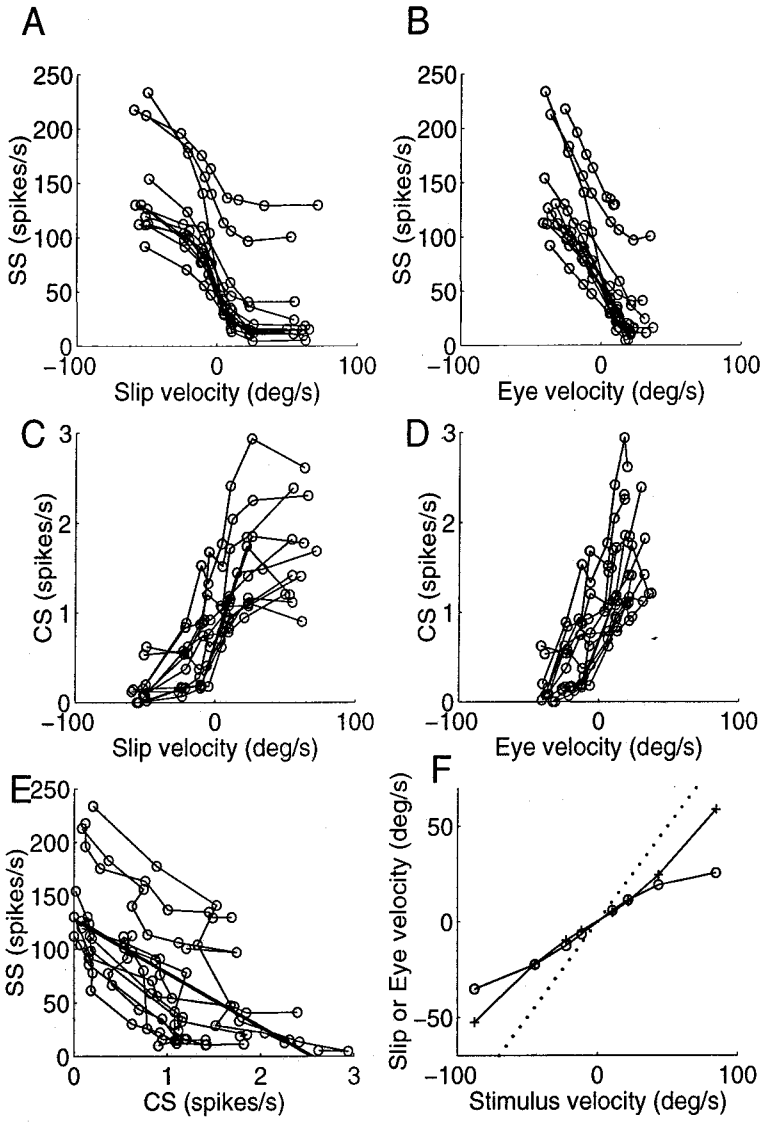

Figure 4.7: Velocity tuning curves of SS and CS. The following relations are shown; (A) SS firing rate and retinal slip velocity, (B) SS firing rate and eye velocity, (C) CS firing rate and retinal slip velocity, (D) CS firing rate and eye velocity, (E) SS and CS firing rate. The bold solid line shows the regression line of all the data. (F) The retinal slip velocity (circle) as a function of the stimulus velocity, and the eye velocity (cross) as a function of the stimulus velocity. The dotted line shows the line with a slope of 1.0 and passing through the origin. Retinal slip was calculated by subtraction of eye movement from stimulus movement. Upward or contralateral motion was assigned positive polarity. Each set of data points connected by a line represents data from an individual cell (n=12).

mean SS firing rate was approximately a linear function of the eye velocity (Figure 4.7B). The correlation coefficient between the mean SS firing rate and eye velocity for each of 12 cells was calculated and then averaged (mean = -0.99). The absolute value of the mean correlation coefficient (-0.91) between the SS firing rates and the slip velocities was statistically significantly smaller (P=0.0001) than that between SS and eye velocity. This observation provides quantitative evidence that the relationship between the SS firing rate and eye velocity is more linear than the relationship between the SS firing rate and slip velocity.

The mean CS firing rate of each cell was approximately an increasing, saturating function of the slip velocity, although some exceptions can be seen especially at large slip velocities (Figure 4.7C). At stimulus velocities between 40 and 80 deg/s, some cells exhibited an increase, some a decrease, and some no change in CS firing rate. As found for SS (Gomi et al. 1998), the relationship between the mean CS firing rate and the eye velocity was more linear (Figure 4.7D). The mean correlation coefficient between CS firing rate and eye velocity (0.93) was statistically larger than (P=0.008) that between CS firing rate and slip velocity (0.89), again providing quantitative evidence that the relationship between CS firing rate and eye velocity is more linear than the relationship between CS firing rate and slip velocity.

The correlation coefficient between the mean SS and CS firing rate at each stimulus velocity was calculated for each of 12 cells (Figure 4.7E) and then averaged (mean = -0.91, SD = 0.06; P=0.05). This result demonstrates that there is a reciprocal relationship between the mean SS firing rate and the mean CS firing rate with respect to their stimulus and eye velocity dependence. The very large negative slope (-48.2) of the regression line in Figure 4.7E for the average data of 12 cells indicates that modulation of CS firing rate depending on different stimulus speeds was opposite in sign and only 2.1 % of that of SS.

SS and CS dependencies on either the slip velocity or the eye velocity were examined in Figure 4.7A-D. Because OFR is essentially induced by the retinal slip, one may wonder that the slip velocity is very highly correlated with the

resultant eye velocity, thus the above analyses might not be sensible. Plotting the averaged slip velocity (cross) and the averaged eye velocity (circle) as functions of the stimulus velocity resolved this issue (Figure 4.7). Despite the small stimulus velocity range (from -40 deg/s to 40 deg/s), the two curves had opposite curvatures. Furthermore, for the largest stimulus speeds (-100 and 100 deg/s), the eye velocity showed clear signs of saturating while the retinal slip kept increasing. Thus, even for the averaged behavior, the retinal slip and the eye movement were considerably different. Marked differences in their transient behaviors will be given below.

4.4 Temporal patterns of CS firing rates

In V cells (n=9), the SS firing rate decreased and the CS firing rate increased in response to upward 80 deg/s stimulus motion (Figure 4.8A). Moreover, CS and SS of an individual cell appeared to be affected to similar extents by the same stimulus motion (e.g., cells 1 and 2 exhibited relatively small changes in both CS and SS firing rate, while cell 3 exhibited relatively large changes in both CS and SS firing rate). Furthermore, although the percent change in the SS firing rate was much larger than that of CS (note the 10 times difference in ordinate scales between the left and right columns), the SS temporal firing profiles were similar to those of CS if the sign was reversed and the magnitude scaled.

There was a significant cell-to-cell negative correlation (-0.76, P=0.01) between the mean magnitude of change from the spontaneous activity in the SS and CS firing rates in response to upward 80 deg/s stimulus motion (Figure 4.8B). This result statistically supports the above qualitative observation suggesting that the magnitude of change in the CS firing rate parallels the magnitude of change in the SS firing rate. Because the slope of the regression line is -17.9, the population mean change in CS firing rate is 5.6 % of that of SS, for the preferred direction of CS and the anti-preferred direction of SS. The Y-axis intercept of the regression line (Figure 4.8B) was not significantly different from zero (P=0.23), which suggests that the SS firing rate is unmodulated if the CS firing rate is unmodulated and vice versa.

There was a statistically significant negative correlation ($P = 0.0001$) between the instantaneous CS and SS firing rates within the same 2 ms time bin (Figure 4.8C) for cell 1 shown in Figure 4.8A. The instantaneous SS and CS firing rates were negatively correlated for all nine cells examined in Experiment 3. For seven of the nine cells, the negative correlation was statistically significant ($P < 0.01$). This analysis provides statistical evidence that the SS temporal firing profile is similar but of opposite sign to the CS temporal firing profile.

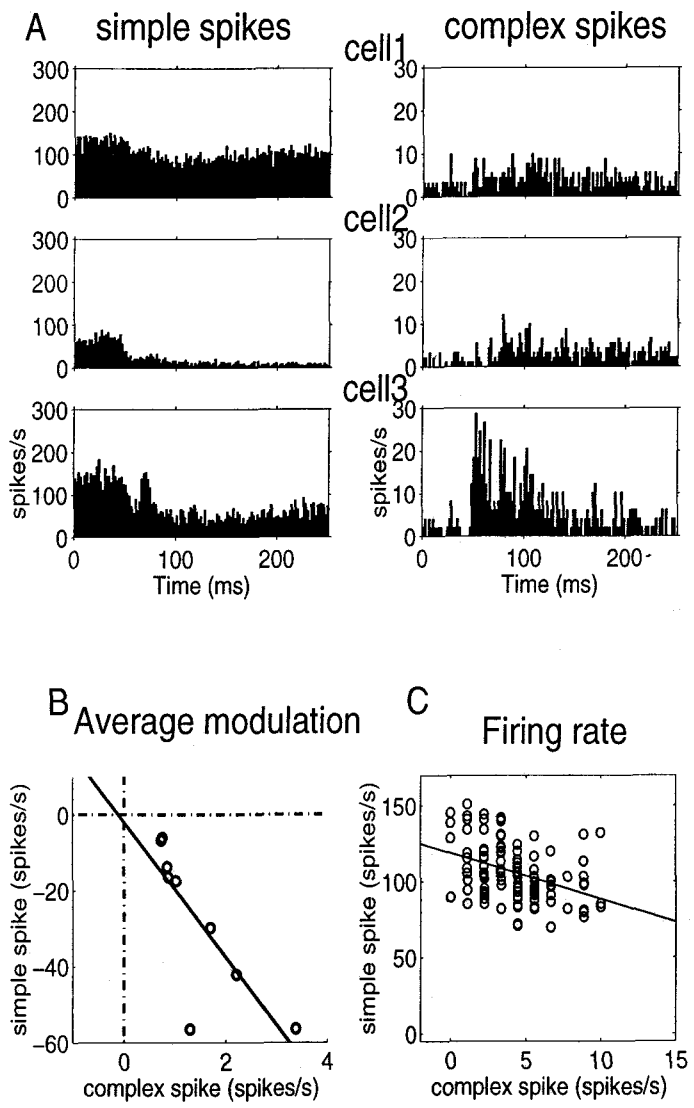

Figure 4.8: Reciprocal relationships between the CS and SS firing rates. (A) The SS and CS firing rates evoked by upward stimulus motion at 80 deg/s (1 ms bins from 0 to 300 ms after the onset of stimulus motion) for three example cells. (B) The mean percent change in SS firing rate for each cell is plotted against that of CS. The solid line represents the linear regression of the data. (C) The instantaneous SS firing rates (binned in 2 ms intervals from 0 to 300 ms after the onset of stimulus motion) of cell 1 shown in A were plotted as a function of those for CS in the same time bins. The solid line represents the linear regression of the data (n=150; r=-0.38; P=0.0001).

4.5 Examination of generalized linear model for firing data

Test of binomial distribution of spike counts

In this section we confirmed the justification of application of generalized linear model for firing probability. First, the binomial distribution of the spike counts was examined. Figure 4.9 shows the data sampling method for testing the binomial distribution.

First, 10 traces of data were randomly sampled from 327 trace data of SS and CS. We made 200 times random sampling of 10 traces. Then we analyzed the relationship between mean and variance of spike counts for each time bin in 200 data. If total spike counts in each time bin Y obey binomial distribution, the following relationship between mean $E[Y]$ and variance $V[Y]$ should be observed. p means probability, N means trial number.

$$E[Y] = Np \tag{4.2}$$

$$V[Y] = Np(1-p) = E[Y](1 - \frac{E[Y]}{N}) \tag{4.3}$$

In Figure 4.10, the relationship between mean and variance in SS and CS are shown. If binomial distribution of $N = 10$ occurs, then $V[Y] = E[Y](1 - \frac{E[Y]}{10})$. Lines in the Figure indicate theoretical value, and the actual data were plotted by $*$. For both SS and CS, actual data were distributed uniformly around theoretical value. That indicates the data obey binomial distribution in individual time bin.

In analyzing the instantaneous firing probability, the spike discharge should be occurred independently of neighboring spikes. Figure 4.11 shows auto-correlation of SS (A) and CS (B). These figure indicate within the range of refractory period of spike (about 3 ms), no spikes were observed. And uniform auto-correlation was observed beyond the refractory period. Consequently, the independency of spike firing was confirmed.

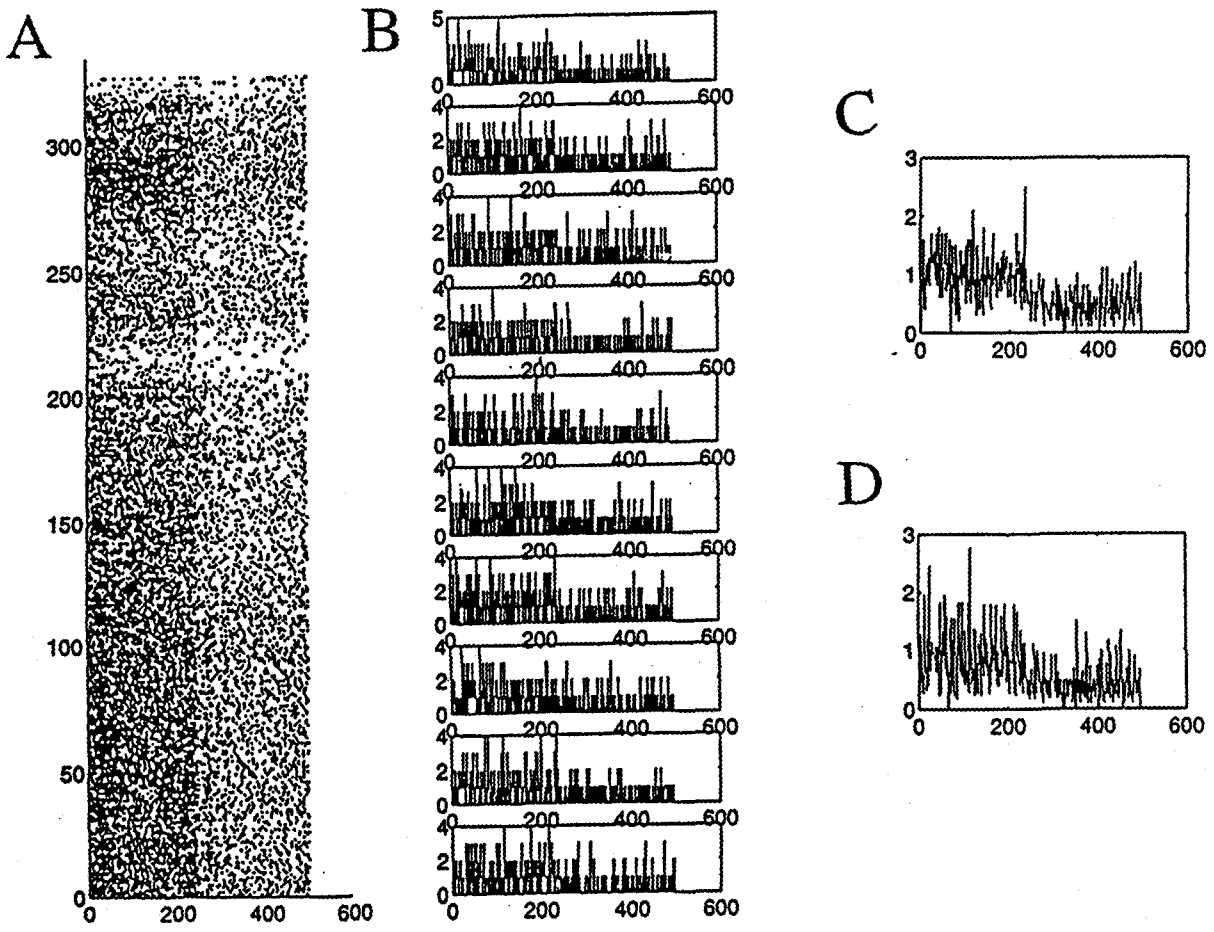

Figure 4.9: Data sampling for confirming the binomial distribution of spike counts (A) Rastergrams of spike firing, (B) Total spike counts in randomly sampled 10 traces. (C) Mean of 200 random data for each time bin, (D) Variance of random 200 data for each time bin

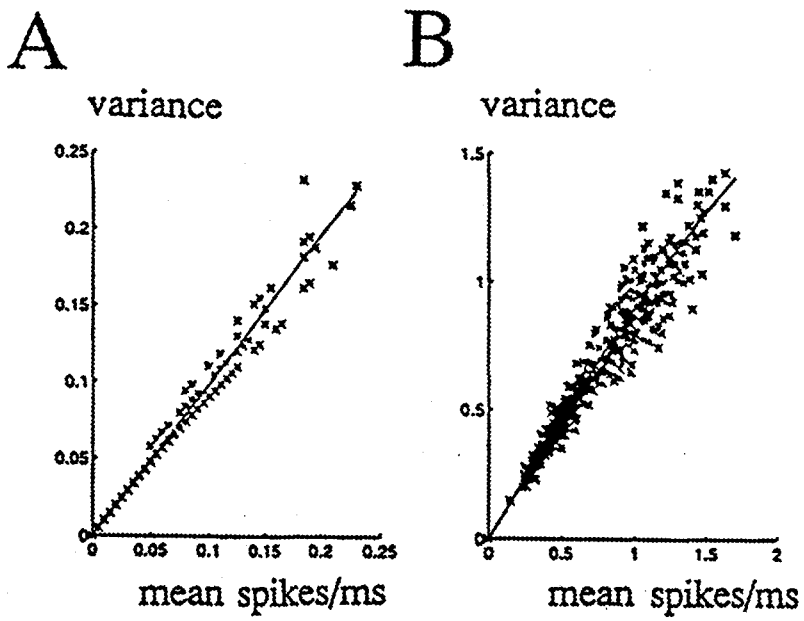

Figure 4.10: The mean and the variance of spike counts. (A)Data in CS, (B) data in SS.

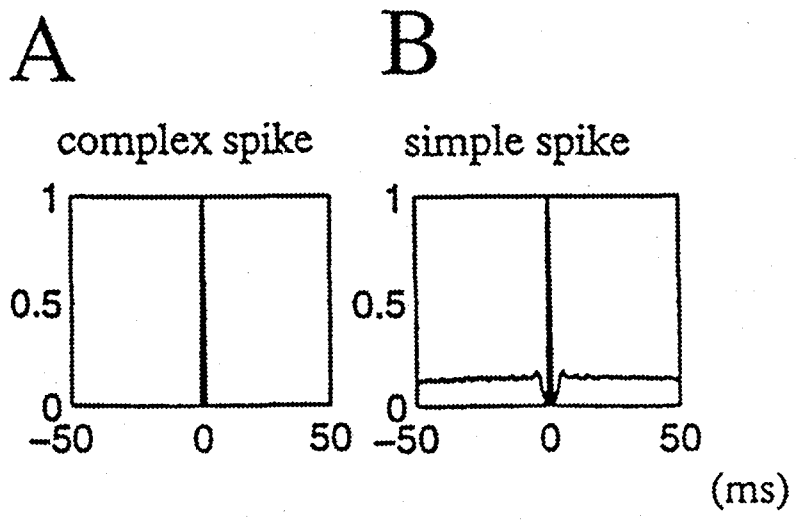

Figure 4.11: Auto-correlation for CS (A) and SS (B).

Problems in using the minimum squared error method

Figure 4.12 shows the result of reconstruction in SS and CS by the linear summation of eye accerelation, velocity and position using the minimum squared error method.

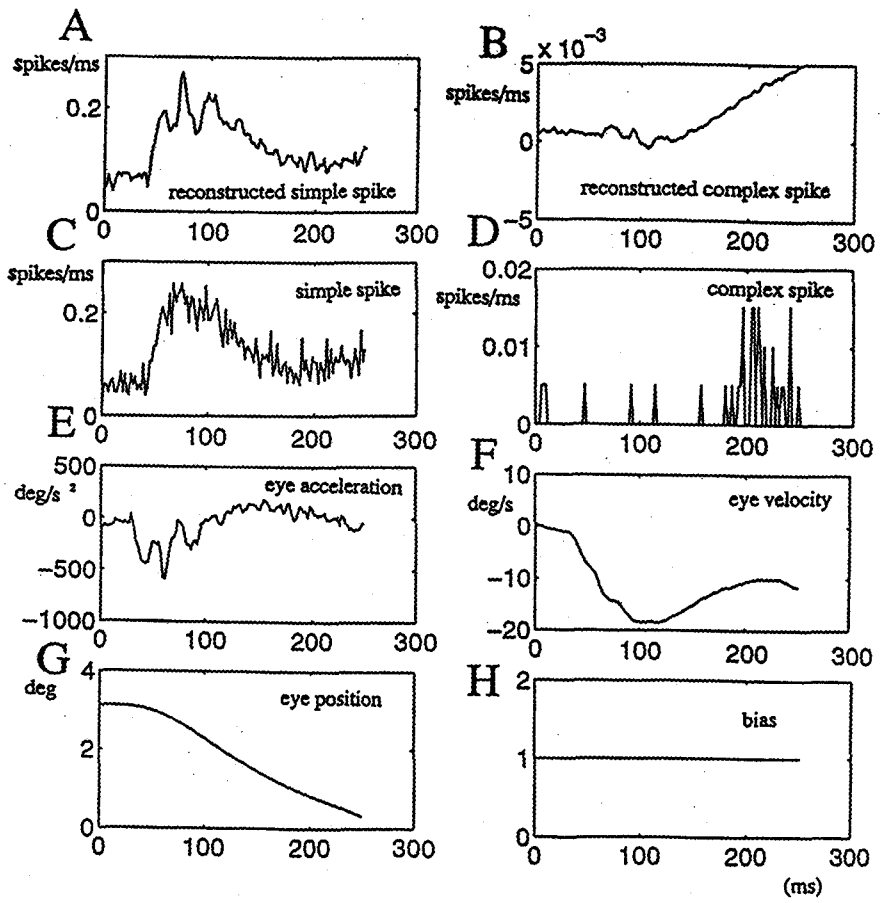

Figure 4.12: Reconstruction using the minimum squared error method. Trial number was 99 for both SS and CS.

The coefficient of determination (square of correlation coefficient) in SS was 0.76. However that of the CS was 0.18. The low coefficient of determination in CS was derived from large sampling noise in binomial distribution of low

probability. The reconstruction was also inappropriate because reconstructed firing rate had negative (less than zero) component.

Then we reconstructed the same data by a generalized linear model. the results were shown in Figure 4.13. No negative components were found in estimated probabilities.

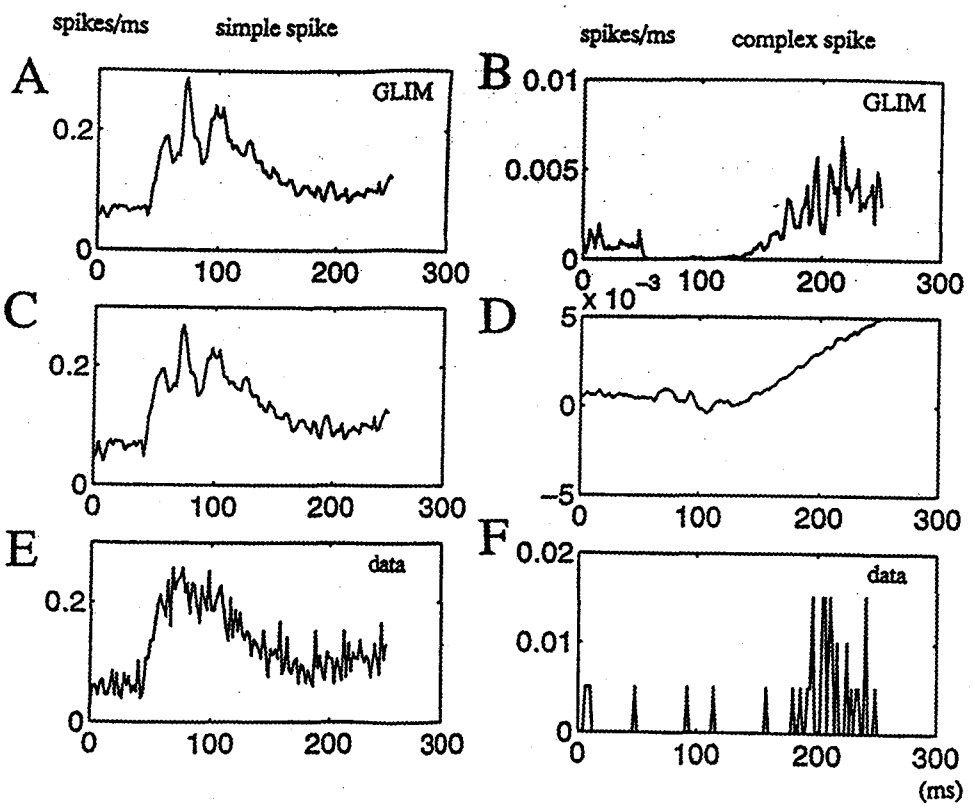

Figure 4.13: Comparison of reconstruction between generalized linear model and normal linear model. (A) SS modeled by generalized linear model, (B) CS modeled by generalized linear model, (C) SS modeled by normal linear model, (D) CS modeled by normal linear model,

Comparison of variance between residual error and intrinsic error derived from binomial distribution

We examined relationship between actual data and residual error in the reconstruction using generalized linear model. If the reconstruction is good, the variance of residual error is approximately the same as the intrinsic variance in binomial distribution given by estimated probability p and trial number N.

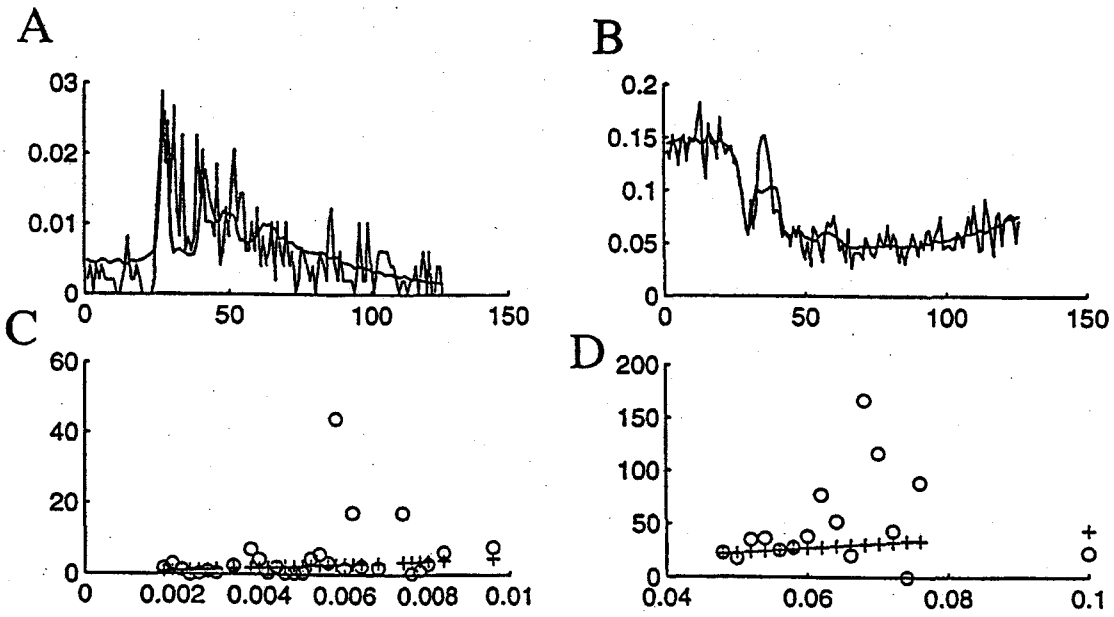

Figure 4.14: Residual error in SS and CS. (A), (B) shows actual data and reconstructed probabilities. In (C), (D) horizontal axes show mean of probability, vertical axes show variance of data. (o) shows the actual data, and (+) shows theoretical value from binomial distribution N=312.

Figure 4.14A and B shows reconstructed data by generalized linear model and actual data of SS and CS. (o) indicates the mean of probability and variance of residual error every 0.0001 step of estimated probability (C) and every 0.001 steps (D) of the estimated probability. + in Figure 4.14 shows theoretical value of mean and variance calculated from binomial distribution N=312. The variance of residual error uniformly distributed around the variance of binomial distribution. Thus the variance of residual error is similar to that of binomial distribution. The mean of (variance of the residual error)/(variance of binomial distribution) is 1.91 in SS and 1.70 in CS. The approximation of SS and CS were similar. Although figure was not shown, auto-correlation of residual error was zero around 0 ms.

Estimation of goodness-of-fit by deviance

The relationship between degree of approximation and trial number or firing rate was examined by simulation. The data composed of various kinds of trial numbers were artificially generated. The data generation was based on the binomial distribution and based on an actual estimated probabilities of SS and CS (327 trials in each). We made 100, 200, 300, 500 trials data. Ten data set was made for individual trial numbers.

The determination coefficients increased with increase in trial number in SS and CS in Figure 4.15. However, the determination coefficient in CS with 1000 trials was approximately equal to that of the SS with 50 trials. Theoretically, if the firing rate is 1/p times, p times trials are necessary to obtain the same degree of coefficient determination. Then, the same data were estimated by generalized linear model and the deviances in SS and CS were compared. The degree-of-fit did not coupled with either trial number or firing rate in Figure 4.16.

The confidence intervals of model parameter (coefficient for eye acceleration) in SS and CS were shown in Figure 4.17.

The magnitudes of confidence intervals decreased with increase in the trial number. Figure 4.17B shows, in parameter estimation of the CS, about 200

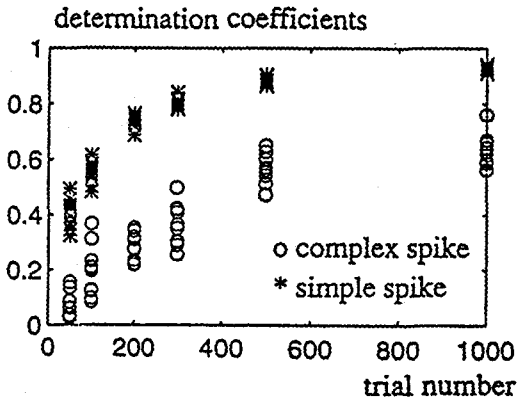

Figure 4.15: Coefficient of determination in CS and SS. means that for SS, and ∘ means that for CS.

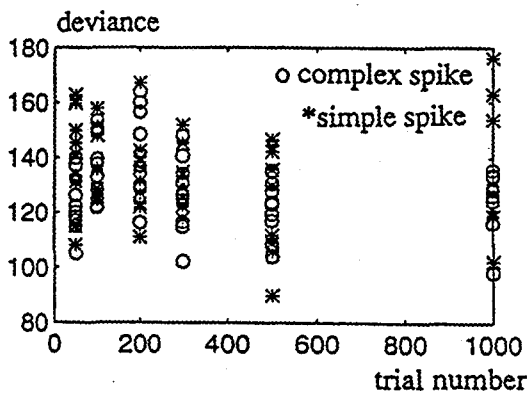

Figure 4.16: Deviance in SS and CS

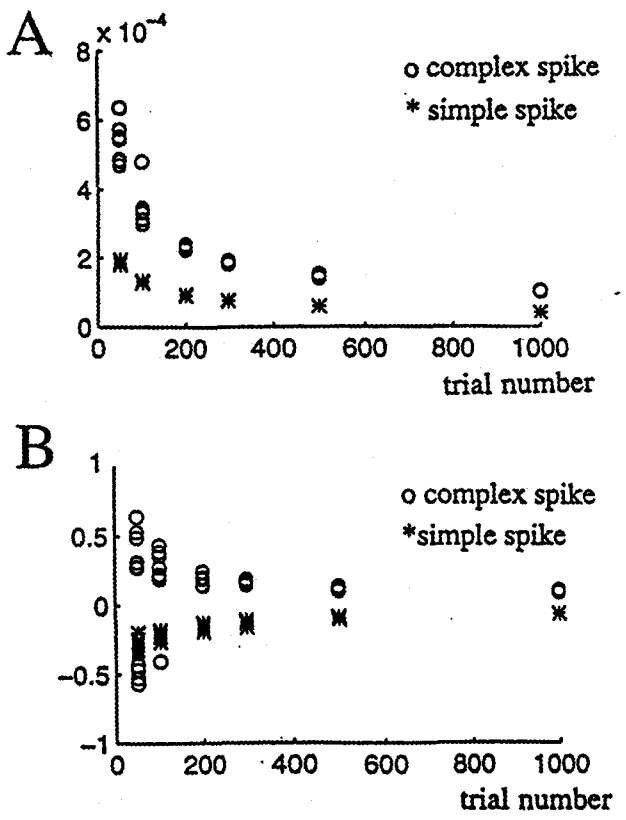

Figure 4.17: (A) Confidence interval of accerelation coefficient of SS $*$ and CS $\circ$. (B) The confidence intervals were divided by coefficients themselves.

trails was sufficient for obtaining good estimation as SS.

4.6 Reproduction of firing probability of CS

The result of using a generalized linear model of eye movement to reproduce the SS and CS firing probability for five in Experiment 3 is shown in Figure 4.18 for five individual cells. The mean correlation coefficient between the observed firing rate and the estimated firing probability was 0.84 ± 0.12 for SS and 0.48 ± 0.10 for CS for the nine cells in Experiment 3.

The mean deviance of the CS firing probability for the eye movement model (Equation 3.2) was smaller than that of the SS (Table 1) indicating that the CS firing probability was more accurately reproduced than that of the SS. Furthermore, the deviance of the CS firing probability was smaller than that of the SS firing probability on an individual cell basis for seven of the nine Purkinje cells analyzed. As the number of trials performed while recording from a single cell approaches infinity, the firing rate (spikes/s) multiplied by the time bin (s) should approach the firing probability p. On the other hand, if the trial number n is finite, there are large fluctuation in firing rate with a standard deviation $\sqrt{np(1-p)}$ due to the binomial distribution (see Methods). Thus, the rapid fluctuation of the firing rate from the predicted firing probability observed in Figure 4.18 is not mainly an error due to the model, but rather sampling noise inherent to the stochastic spike-count data itself.

A generalized linear model of eye movement was also used to reproduce the SS and CS firing probability from Experiment 2. A single set of parameters was estimated for each cell to reproduce the firing patterns for all stimulus velocities. Figure 4.19 shows the result of using a generalized linear model to reproduce the SS and CS firing probability from the eye movement for five individual cells in Experiment 3.

As in Experiment 3, the mean deviance of the CS firing rate was smaller than that of the SS (Table 1) and the deviance of the CS firing rate was smaller than that of the SS firing rate for all 12 individual cells recorded in Experiment 2. Thus, these data also indicate that the CS firing probability was better reproduced from eye movement than was the SS firing probability.

The mean correlation coefficient between the observed firing rate and the

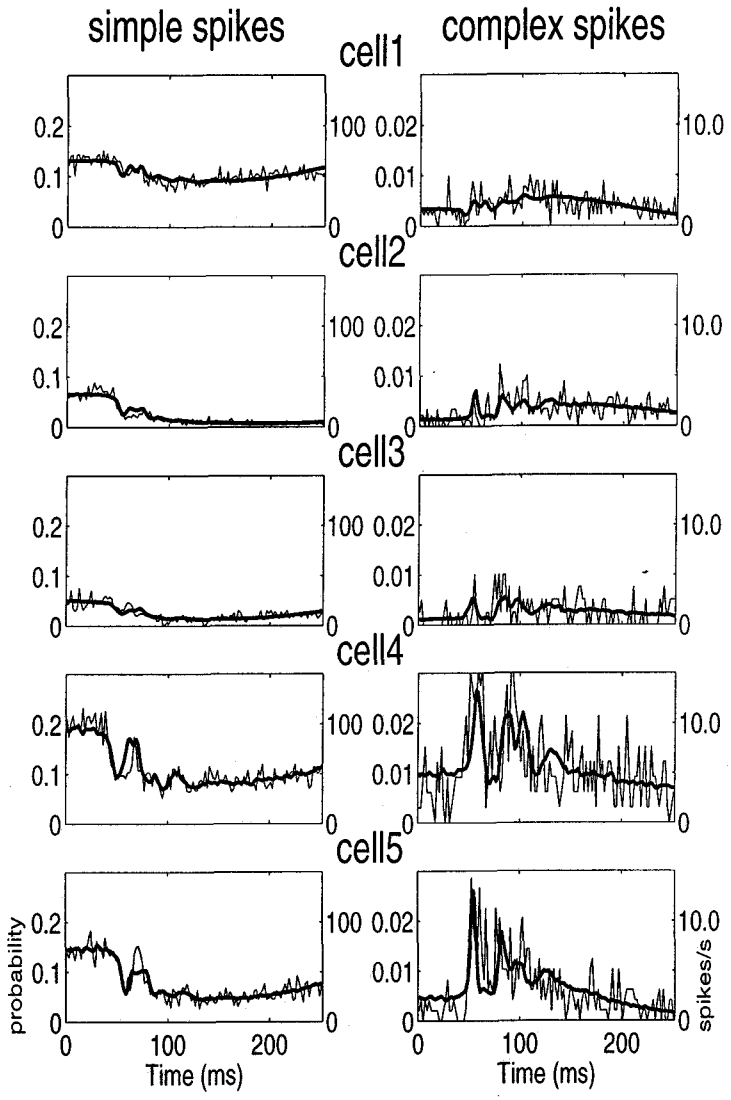

Figure 4.18: Reproduction of the SS (left) and CS (right) firing probability from the eye movement for five example V cells in response to upward stimulus motion at 80 deg/s using a generalized linear model. The thin curves show the observed firing rate in 2 ms bins, and the thick curves show the estimated firing probability within the corresponding time bin. Note that the ordinate scales for the firing rate (right) and the firing probability (left) were matched such that the asymptote of the former overlaid that of the latter. Accumulated trial numbers for the five cells were 901, 899, 396, 327, and 487 from top to bottom. The data are shown from top to bottom in order of increasing mean change in firing rate in response to stimulus motion.

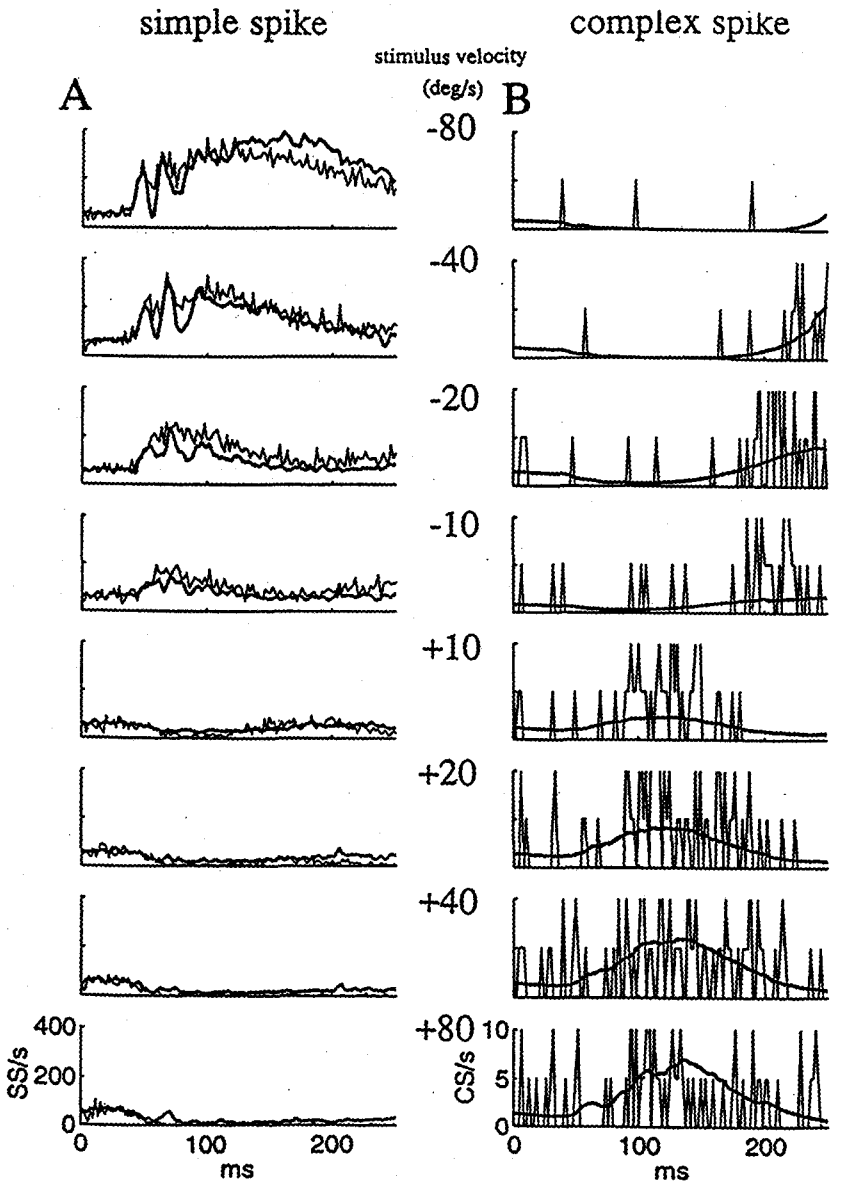

Figure 4.19: Reconstruction of multiple SS and CS data with eye movement model by a single set of parameters. Several vertical stimulus (+80, +40, +20, +10, -10, -20, -40, -80 (deg/s)) was applied, and all of the data were modeled by a single set of parameters in SS (A) and CS (B) Trial numbers were 95 for individual traces.

estimated firing probability was 0.84 ± 0.12 for SS and 0.48 ± 0.10 for CS for the nine cells. The mean deviance was smaller for the CS firing probability (Table 4.1) indicating that the CS firing probability was more accurately reproduced from eye movements than was that of SS. Furthermore, the deviance was smaller for the CS firing probability than the SS firing probability on an individual cell basis for seven of the nine Purkinje cells analyzed. As the number of trials performed while recording from a single cell approaches infinity, the firing rate (spikes/s) multiplied by the time bin (s) should be equal to the firing probability p. On the other hand, if the trial number n is finite, there are large fluctuations in firing rate with a standard deviation $\sqrt{np(1-p)}$ due to the binomial distribution. Thus, the rapid fluctuation of the observed firing rate from the predicted firing probability observed in Figure 4.18 is not error due to the model, but rather sampling noise inherent to the stochastic spike-count data itself.

A generalized linear model of eye movement was also used to reproduce the SS and CS firing probability from Experiment 2. A single set of parameters was estimated for each cell to reproduce the firing patterns for all stimulus velocities. As in Experiment 3, the mean deviance of the CS firing rate was smaller than that of the SS (Table 1) and the deviance of the CS firing rate was smaller than that of the SS firing rate for all 12 individual cells recorded in Experiment 2. Thus, these data also indicate that the CS firing probability was better reproduced from eye movement than was the SS firing probability.

We examined whether temporal patterns of firing probability in SS and CS encode significantly sensory or motor information. The firing probabilities of CS and SS were reconstructed via the generalized linear model of eye movement (Equation 3.2) or retinal slip (Equation 3.6), then the deviances were compared between the eye movement model and the retinal slip model. To improve the data reliability, we averaged the data from 9 cells recorded in Experiment 3 as shown in Figure 4.20. Because of this population averaging, the stochastic noise in the firing rate of CS was reduced. The temporal patterns of retinal slip position, velocity and acceleration and eye position, velocity and acceleration

and SS and CS elicited by upward 80 deg/s stimuli are shown in Figure 4.20. Thick lines in G and I show the firing probability reconstructed for SS and CS respectively by the generalized linear model of the retinal slip. Thick lines in H and J show the firing probability reconstructed by the generalized linear model of eye movement for SS and CS respectively.

It may superficially appear that the temporal patterns of the retinal slip and the eye movement are similar and thus that it is statistically difficult to discriminate which signal better reconstructs the firing frequency patterns. But actually even the position temporal patterns are quite different between the two signals unless an appropriate time shift is introduced, while the velocity and acceleration are entirely different with negative correlations. The firing data was best modeled by retinal slip about 40 ms time delayed, and it was modeled best by the eye movement about 10 ms time advanced. Thus, for estimating statistically the extent of similarity of the two signals, we first time delayed the retinal slip by 40 ms and time advanced the eye movement by 10 ms, and then calculated the correlation of the two signals. The correlation coefficient between retinal slip acceleration 0 to 200 ms after onset of the stimulus motion and eye acceleration 50 to 250 ms from onset of the stimulus motion was -0.012. Thus the acceleration patterns were little correlated. The correlation coefficient between velocity of retinal slip and velocity of eye movement was -0.60. Thus the velocity patterns were negatively correlated. The coefficient for position was 0.97. Thus, in summary, the position patterns were highly positively correlated, but the dynamic components (acceleration and velocity) of the two temporal patterns were entirely different.

Comparison of the deviances for the eye movement model and the retinal slip model, as shown in the left two columns of the Table 1 indicates that the SS and CS firing probabilities were reproduced as well or better from the retinal slip than from eye movement for the upward 80 deg/s stimulus in Experiment 3.

But we do not think this is a statistically important observation. To reliably and more rigorously compare the two statistical models in reproducing

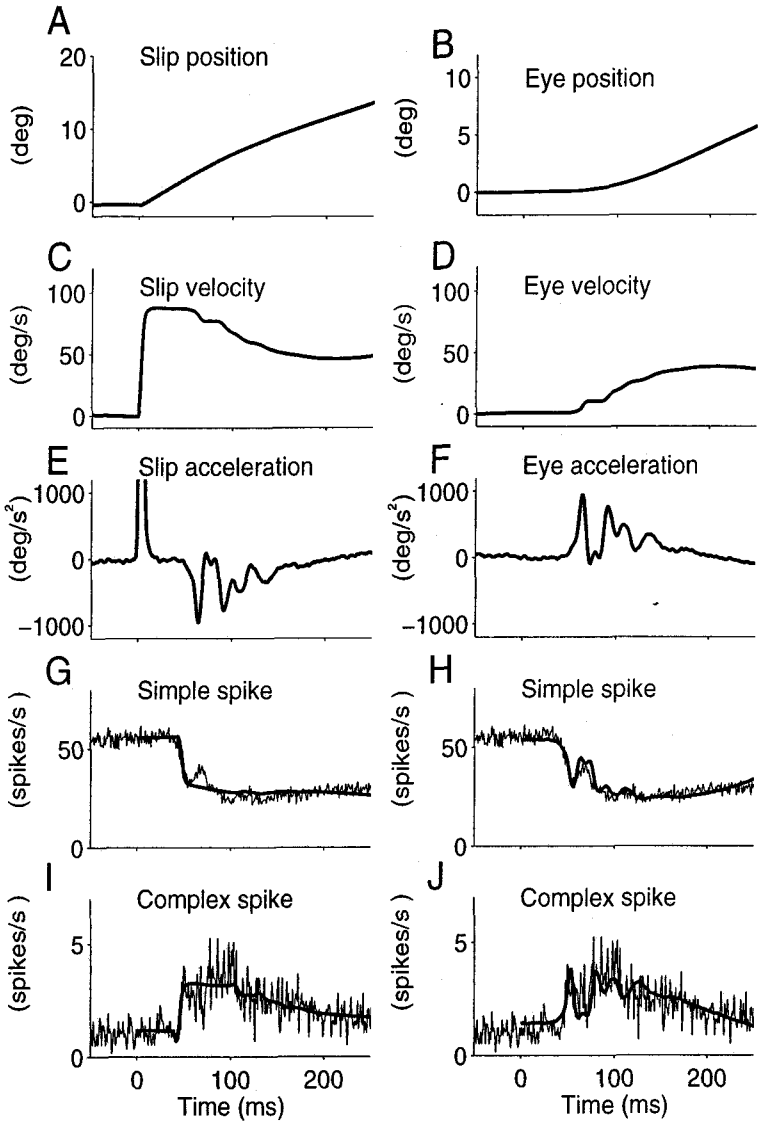

Figure 4.20: Population average of the retinal slip, eye movement, CS and SS of 9 cells in Experiment 3 (5214 trials). The left column shows retinal slip position (A), velocity (C) and acceleration (E) in responses to 80 deg/s upward stimulus motion, and the right column shows eye position (B), velocity (D) and acceleration (F) responses to the same stimulus motion. G and H: thin traces show the population average of firing probability of SS. Thick traces in (G) and (H) show the estimated firing probability of SS from retinal slip and eye movement, respectively. I and J: thin traces show the population average of firing probability of CS. Thick traces in (I) and (J) show the estimated firing probability of CS from retinal slip and eye movement, respectively.

	eye movement Upward 80 deg/s stimulus	retinal slip Upward 80 deg/s stimulus	eye movement 8-speed stimuli	retinal slip 8-speed stimuli
SS	191.3 (88.0)	171.6 (53.9)	358.5 (150.5)	423.4 (183.4)
CS	150.9 (24.1)	138.5 (11.4)	78.5 (11.3)	83.0 (12.9)

Table 4.1: Comparison of mean deviances (± SD) in estimations of firing probability from eye movement and retinal slip. The two left columns show the results from Experiment 3 ,which utilized 80 deg/s stimulus in the preferred direction for CS, and the right two columns show the results from Experiment 2, which utilized 8 or 6 speed stimuli in both the preferred and anti-preferred directions for CS and SS.

the experimental data, the generalization capability of the models should be tested using the data from Experiment 2 because a large variety of stimuli and responses are essential to test the goodness of the models. The mean deviances in Experiment 2 are shown in the right two columns of Table 1. Here, both the SS and CS were better reproduced from the eye movement than the retinal slip. Instead of directly comparing the deviance values themselves, an index of the sensory-motor nature of the signals was calculated as the deviance for the eye movement divided by that for the retinal slip. If the index is smaller than 1, the signal will be more motor in nature, while if it is larger than 1, the signal will be more sensory. First, because the mean of the index for CS (0.95) was close to 1, CS were equally well reproduced from either the retinal slip or the eye movement. Second, the mean of the index for SS (0.85) was smaller than that for CS suggesting that SS are more motor in nature than CS, (and conversely, that CS are more sensory in nature than SS).

The generalized linear model of the eye movement shown in Equation 3.2 nonlinearly transforms the linear weighted summation of the eye acceleration, eye velocity, eye position and the constant term, $M \cdot \ddot{\theta}(t+\delta) + B \cdot \dot{\theta}(t+\delta) + K \cdot \theta(t+\delta) + C$ by the sigmoid function S defined in Equation 3.3. The bold solid curves in Figure 4.21A and B denote this summation, that is the argument of S, or the contents of the square bracket in Equation 3.2 for the SS and CS, respectively. Here, we use the same population data from the 9 cells in Experiment 3, which were already shown in Figure 4.20B, D, F, H and J. The noisy curves denote the inverse of the sigmoid function of the actual firing data: $S^{-1}(y_i/m) = log[(y_i/m)/(1-y_i/m)]$. Because the bold solid curve $S^{-1}(p)$ well approximates this noisy curve, the good fit of the generalized linear model was reconfirmed. The four thin solid curves shown in Figure 4.21A and B indicate the four terms, i.e. $M \cdot \ddot{\theta}(t+\delta)$, $B \cdot \dot{\theta}(t+\delta)$, $K \cdot \theta(t+\delta)$ and C for the SS and CS, respectively. C of the CS was smaller than that of the SS by approximately 4, indicating that the spontaneous firing rate of the CS was about exp(-4) = 0.02 times of that of the SS. The acceleration, velocity and position curves of the CS shown in B had the opposite polarity but similar magnitudes to those

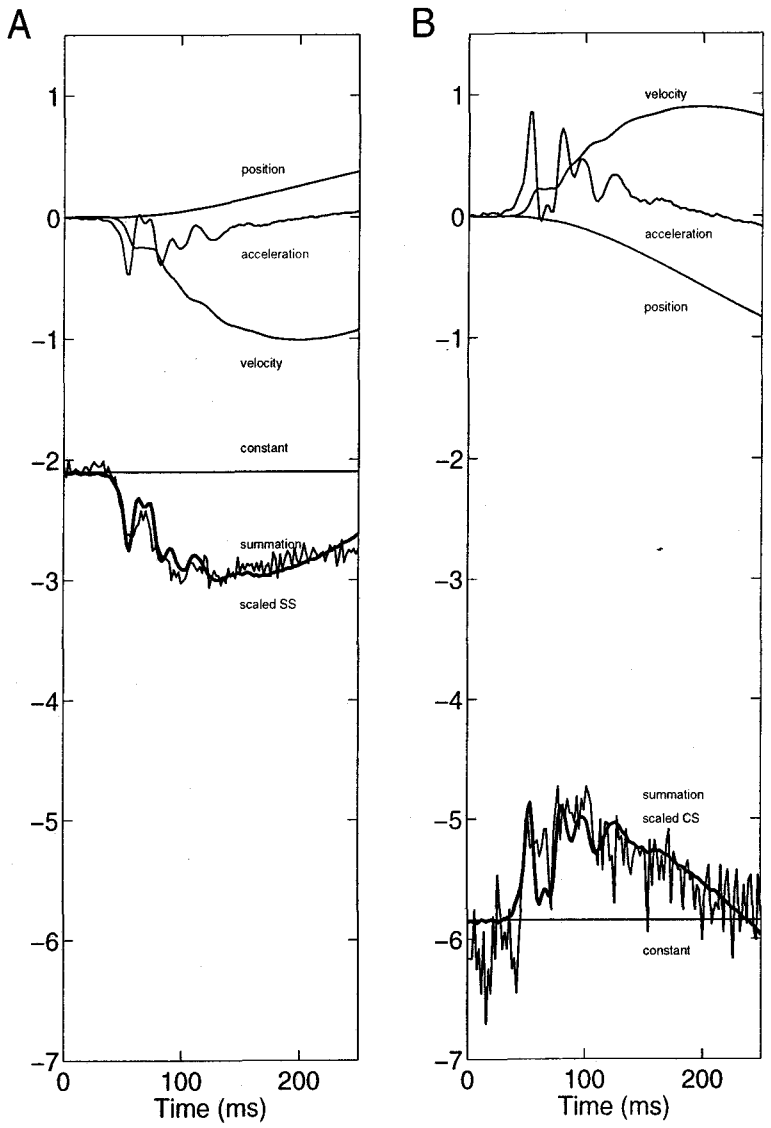

Figure 4.21: The bold solid curves in (A) and (B) indicate the linear weighted summation of the eye acceleration, eye velocity, eye position and the constant term, $M \cdot \ddot{\theta}(t+\delta) + B \cdot \dot{\theta}(t+\delta) + K \cdot \theta(t+\delta) + C$ for the SS and CS, respectively. The four thin solid curves shown in (A) for the SS and in (B) for the CS indicate the four terms in these summations. The noisy curves indicate the inverse of the sigmoid function of the actual firing rates. We use the same aggregated data from the 9 cells in Experiment 3, which were already shown in Figure 4.20B, D, F, H and J.

of SS in A. This reconfirmed that the temporal patterns of firing frequency for the CS are similar to those for the SS if the sign is reversed and the magnitude is scaled by dividing by exp(-4) = 0.02.

Next, we examined the relative contributions of the three factors (acceleration, velocity and position) in reconstructing the SS and CS temporal profiles by calculating the following variance accounted for (VAF) of the eye acceleration, velocity and position, respectively.

$$VAF_{\mathrm{a}} = 1 - \frac{V[S^{-1}[p(t)] - M \cdot \ddot{\theta}(t+\delta)]}{V[S^{-1}[p(t)]]} \tag{4.4}$$

$$VAF_{\mathrm{v}} = 1 - \frac{V[S^{-1}[p(t)] - B \cdot \dot{\theta}(t+\delta)]}{V[S^{-1}[p(t)]]} \tag{4.5}$$

$$VAF_{\mathrm{p}} = 1 - \frac{V[S^{-1}[p(t)] - K \cdot \theta(t+\delta)]}{V[S^{-1}[p(t)]]} \tag{4.6}$$

The VAF indicates what proportion of the total modulation in the S^{-1} transformed firing frequency could be accounted for by each of the three terms. $V[x]$ denotes the variance of x. A larger VAF indicates a larger contribution of that component. VAF_{a}, VAF_{v} and VAF_{p} for the SS were 0.05, 0.51 and -0.55, respectively. VAF_{a}, VAF_{v} and VAF_{p} for the CS were 0.34, -0.24 and -0.29, respectively. These results indicate that the eye velocity component was the most dominant in the SS and eye acceleration component was the most dominant in the CS.

The ratio of the velocity and acceleration coefficients ($\frac{B}{M}$) in the generalized linear model of eye movement (Equation 3.2) for the population data shown in Figures 4.20 and 4.21 was computed. ($\frac{B}{M}$) for SS was 55 and, that for CS was 26. This confirms that the SS contained the larger velocity component, or the CS contained the larger acceleration component.

In both Experiment 3 and Experiment 2, the mean acceleration, velocity, and position coefficients of eye movement (M, B, K) for CS and SS generally had opposite signs, but were of the same order of magnitude (Table 2). The mean C of CS was smaller than that of SS by approximately 4. This also indicates a lower firing probability of the CS than the SS. Taken together, this indicates that the percent change in the CS firing rate is approximately $\exp(-4) = 0.02$ that of the SS firing rate. The onset of SS and CS modu-

	SS Upward 80 deg/s stimulus	CS Upward 80 deg/s stimulus	SS 8-speed stimuli	CS 8-speed stimuli
M	-0.00051 (0.00048)	0.00093 (0.00061)	-0.00072 (0.00086)	0.0017 (0.0012)
B	-0.036 (0.020)	0.023 (0.017)	-0.036 (0.010)	0.049 (0.039)
K	0.10 (0.096)	-0.14 (0.11)	0.078 (0.0071)	-0.22 (0.34)
C	-2.2 (0.62)	-5.9 (0.67)	-2.4 (0.62)	-6.5 (1.1)
δ (ms)	10.4 (4.9)	6.2 (10.2)	11.0 (6.9)	4.2 (10.7)

Table 4.2: Comparison of estimated model parameters in the generalized linear model of eye movement described in Equation 3.2 (means $\pm$ SD) for reconstruction of SS and CS firing probabilities. The left two columns show the results from Experiment 3, and the right two columns show the results from Experiment 2.

lation preceded the onset of eye movement by a similar amount: the average δ (Equation 3.2) from 21 cells from Experiment 2 and Experiment 3 was 5.1 $\pm$ 10.3 ms for CS and 10.8 $\pm$ 6.0 ms for SS (mean $\pm$ SD), (not significantly different $P > 0.05$; see also Table 2). Because M, B, K, C, and δ reflect the temporal firing probability profile, these results indicate that the CS temporal firing probability profile was similar to that of SS if the sign was reversed and the modulation amplitude scaled. Thus, these data provide additional quantitative evidence with high temporal resolution (2 ms bin) that the SS and CS temporal profiles were similar but opposite in sign.

We have demonstrated previously that SS recorded in the VPFL exhibit temporal firing profiles that closely follow an inverse dynamics representation of eye movements, and that the ratio between the acceleration and velocity coefficients is close to that of motor neurons, thus indicating their role as the dynamic motor commands (Shidara et al. 1993; Kawano et al. 1996; Gomi et al. 1997). In the present study, we modeled firing probability by generalized linear models instead of using linear models for firing frequency. Because the sigmoid (logarithmic) function in the generalized linear model can be approximated by an exponential function if its argument is negative and its absolute value is large, the acceleration, velocity, and position coefficients of the linear model can be approximated from the corresponding coefficients of the generalized linear model by multiplying by $\exp(C)$. Thus, the ratio of the coefficients can be directly compared between the linear model and the generalized linear model used in the present study.

The mean velocity and acceleration coefficient ratio of eye movement model ($\frac{B}{M}$) for 21 cells in Experiment 2 and 3 for SS was 56, which is close to that for motor neurons (67) (Keller 1973), thus these results are consistent with the hypothesis that SS provide dynamic motor commands (Shidara et al. 1993; Kawano et al. 1996; Gomi et al. 1997). The mean ratio ($\frac{B}{M}$) for 21 cells in Experiment 2 and 3 for CS was 28. This indicated the temporal profile of SS contained the larger velocity component or that of CS contained the larger acceleration component. The same conclusion was drawn already from appli-

cation of the same model to the accumulated data from 9 cells in Experiment 3 (Figures 4.20 and 4.21). The VAF analysis of the same data also reconfirmed this.

Plots of the best-fit parameters of the coefficients M, B, K, and C for the SS data against the best-fit parameters for the CS data for each of the 21 Purkinje cells from Experiments 2 and 3 indicate that the acceleration, velocity, and position coefficients for the SS and CS data generally had opposite signs (note the quadrant), but were of the same order of magnitude, even on a cell-to-cell basis (Figure 4.22). The regression lines in Figure 4.22A and B were constrained to pass through the origins for the following two reasons. First, the results shown in Figure 7B indicate that SS were unmodulated if CS were unmodulated. This suggests that the inverse dynamics coefficients were zero for both SS and CS, so that the origin was a default data point. Second, the results of Experiment 1 indicate that both CS and SS were unmodulated by the stimulus direction perpendicular to their optimal and anti-optimal directions. Thus, a large number of data points concentrate on the origin. The slopes of the regression lines for M (P=0.02) and B (P=0.00001) were significantly more negative than zero based on a Student's t-test. This result indicates that there are cell-to-cell negative correlations between the SS and CS coefficients, and consequently cell-to-cell negative correlations between the SS and CS temporal firing patterns. M and B are functionally more important than K because SS provide only the dynamic part of the motor commands (Shidara et al. 1993; Kawano et al. 1996; Gomi et al. 1997).

Examination of the model freedom

Using chai-square test, the ability for comparing the degree of the model fit between two nested models were already shown. Thus, we examined the the best combination of parameters (either jerk, acceleration, velocity and position of eye movement or those of retinal slip) for SS and CS. For example, in the case of the eye movement, we used the generalized linear model of (1) only one parameters, (2) combination of two parameters, (3) combination of three

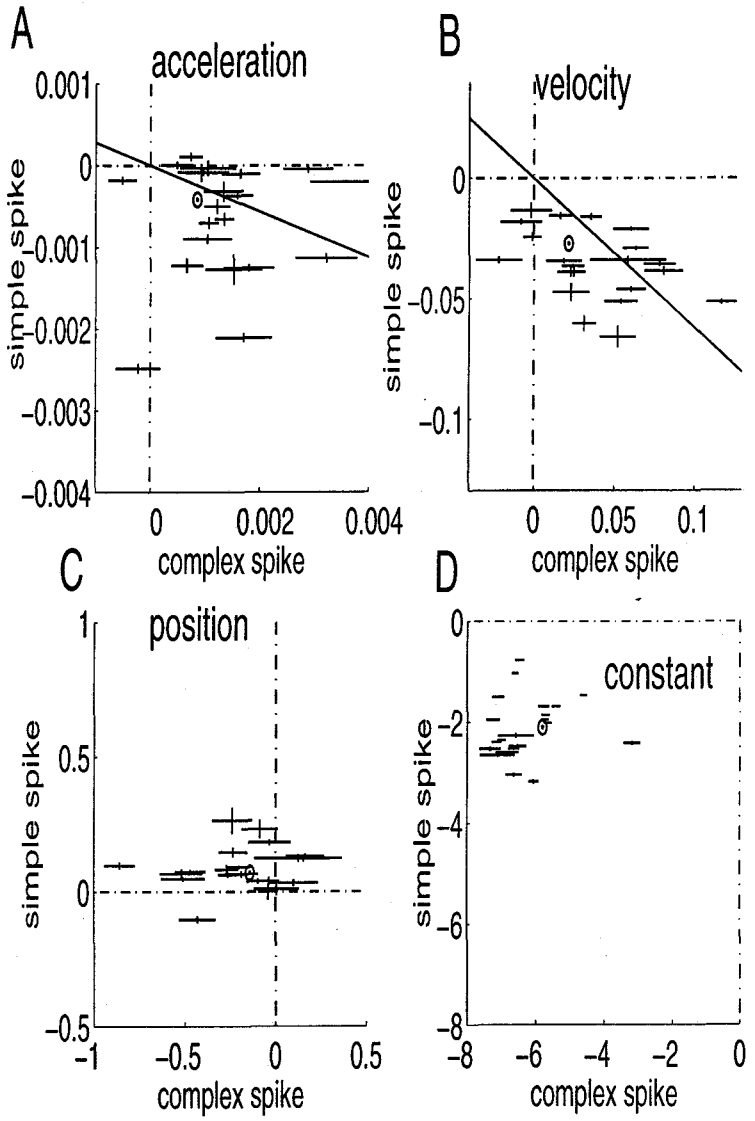

Figure 4.22: The estimated parameters M, B, K, C, and their confidence intervals are shown in A, B, C, and D, respectively. The estimated coefficient for SS of each cell is plotted against that of CS using the same scale for the ordinate and the abscissa. The center of each cross indicates the maximum likelihood estimation, while the lengths of the vertical and horizontal bars indicate the square roots of the asymptotic variance for SS and CS, respectively. The crosses represent data from nine cells responding to upward stimulus motion at 80 deg/s and data from 12 cells in which six or eight different velocities were used. The estimated coefficients from the averaged data to upward stimulus motion at 80 deg/s (5214 trials) are plotted as double circles.

parameters and (4) combination of all of four parameters. When we compared the deviance between two models whose freedom were different, deviances always decrease with increment of model freedom. Since these process depends on chai-square distribution, we added chai-square value (p=0.05) to the deviance with increase of model freedom. The freedom of the chai-square value was equal to the difference of the model freedom. The results ware shown in Table 4.2. The table indicates that,

1. SS was well-modeled by eye movement.

2. CS was well-modeled by retinal slip in Experiment 3, but more general condition (Experiment 2) CS was well-modeled by eye movement.

The results may reflect the motor characteristics of SS. The CS may encode visual related signal in each trials, but in general conditions the characteristics are aligned with eye movement.

A

cell No.	Simple spike		Complex spike	
1	M	-M	M	-K
2	S	+J	S	-K
3	M	-M	S	-K
4	S	-M	S	-K
5	S	+J	S	-M
6	S	-M	S	-M
7	S	-M	S	-M
8	M	-M	S	-K
9	S	+J	S	MBK
10	M	+J	S	-M
11	M	-M	S	-M
alldata	M	+J	S	+J

The result of local fit.

B

cell No.	Simple spike		Complex spike	
1	M	-M	M	-M
2	M	+J	M	-K
3	M	-M	M	-K
4	M	-M	M	-K
5	M	+J	M	MBK
6	M	-M	M	-K
7	M	-M	M	-M
8	S	-M	S	-M
9	M	+J	M	-M
10	S	+J	S	-K
11	M	-M	M	-M
12	M	+J	S	-M

The result of global fit.

Table 4.3: The best model composed of eye movement or retinal slip. The best combination of parameters (either jerk, acceleration, velocity and position of eye movement or those of retinal slip) for SS and CS were shown. (A) shows the result in Experiment 3. (B) shows the result in Experiment 2. M means eye movement model, S means retinal slip model. +J means the model composed with all four parameters, combination of acceleration, velocity, position plus jerk. -M, -B and -K mean models whose parameters were composed of two parameters, combination of acceleration, velocity, position minus acceleration, velocity or position.

4.7 Short-term modulation of SS by CS

The cross-correlation analysis was applied to the SS (Figure 4.23A) and the CS (Figure 4.23B) firing for nine cells presented with upward 80 deg/s stimulus motion (Experiment 3).

Figure 4.23 shows the results for one example cell. The apparent cross-correlation R_{app} was directly calculated by CS spike trigger averaging of the SS (Figure 4.23C). The stimulus-dependent cross-correlation R_{stm} was similarly calculated after shuffling the impulse trains (Perkel et al. 1967; Toyama et al. 1981) (Figure 4.23D). The true interaction (net cross-correlation $R_{\mathrm{net}} = R_{\mathrm{app}} - R_{\mathrm{stm}}$) between SS and CS (Figure 4.23E) was determined by subtracting the stimulus-dependent cross-correlation from the apparent cross-correlation. The proportion of the SS discharge modulation SS_{CS} that is a direct consequence of short-term effect of CS, can be evaluated by the convolution integral of the CS firing pattern with the net cross-correlation obtained above (Figure 4.23F):

$$SS_{\mathrm{CS}}(t) = \int_0^\infty R_{\mathrm{net}}(s) CS(t-s) ds. \tag{4.7}$$

Comparison of the convolution integral of CS (Figure 4.23F) and the SS peristimulus time histogram (Figure 4.23A) indicates that the estimated CS-induced SS modulation was negligible compared with the actual SS modulation; the ratio of the estimated CS-induced SS modulation (averaged over the interval from 0 to 250 ms from the onset of the stimulus motion and after subtraction of the pre-stimulus firing rate) and the actual SS modulation was very small (0.006) (for the nine cells, mean $\pm$ SD = $1.2\times10^{-2}\pm 1.4\times10^{-2}$). It is important not to overestimate the stimulus-dependent pseudo correlation, and consequently, to underestimate the net correlation and the CS-induced SS modulation. The magnitude of the net cross-correlation between SS and CS observed in the present study was approximately the same order of magnitude as in previous observations (30-50 spikes/s firing rate during the pause and 10-30 ms pause duration; Stone and Lisberger 1990b; Sato et al. 1992). Consequently, the reciprocal relationship between SS and CS cannot be explained by a short-term CS-induced SS modulation. A similar conclusion was derived

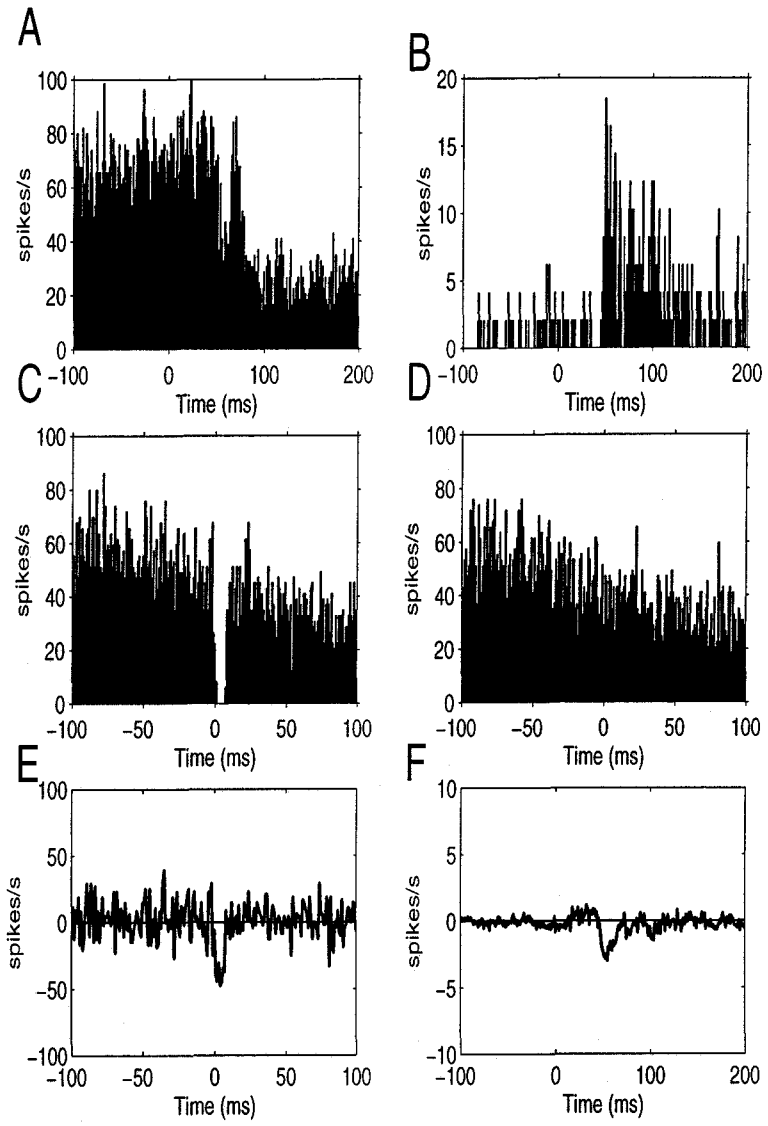

Figure 4.23: The cross-correlation analysis of SS and CS. (A) The SS peristimulus time histogram. (B) The CS peristimulus time histogram. (C) The apparent cross-correlation between SS and CS, R_{app}, which was directly calculated by CS spike trigger averaging of SS. (D) The stimulus-dependent pseudo cross-correlation between SS and CS, R_{stm}, which was similarly calculated after shuffling the impulse trains (Perkel et al. 1967; Toyama et al. 1981). (E) The net cross-correlation between SS and CS, R_{net}, determined by subtracting the stimulus-dependent cross-correlation in D from the apparent cross-correlation in C. (F) The SS modulation, SS_{CS}, which is accounted for by the short-term effect on SS by CS. The data shown in A-F were obtained from responses of one cell to upward stimulus motion presented 487 times at 80 deg/s.

from studies of other species (Simpson et al. 1996).

4.8 The movement with or without CS

Figure 4.24 shows the firing rate of simple spikes and eye velocity with or without CS during the time intervals 0 ms to 300 ms from the onset of the upward 80 deg/s stimulus motion. C, D shows eye velocity and SS with CS (251 trials), E, F shows eye velocity and SS without CS (76 trials). G shows the difference of eye velocity between with and without CS. Figure H shows that of the SS. Broken lines in G, H shows the level mean $\pm$ 3SD. I, J shows the result of the same analysis from the data which all of the SS and eye velocity trials were randomly shuffled. No difference was observed between actual and shuffled data. We had additional results that the CS itself did not effect on either SS or eye movement.

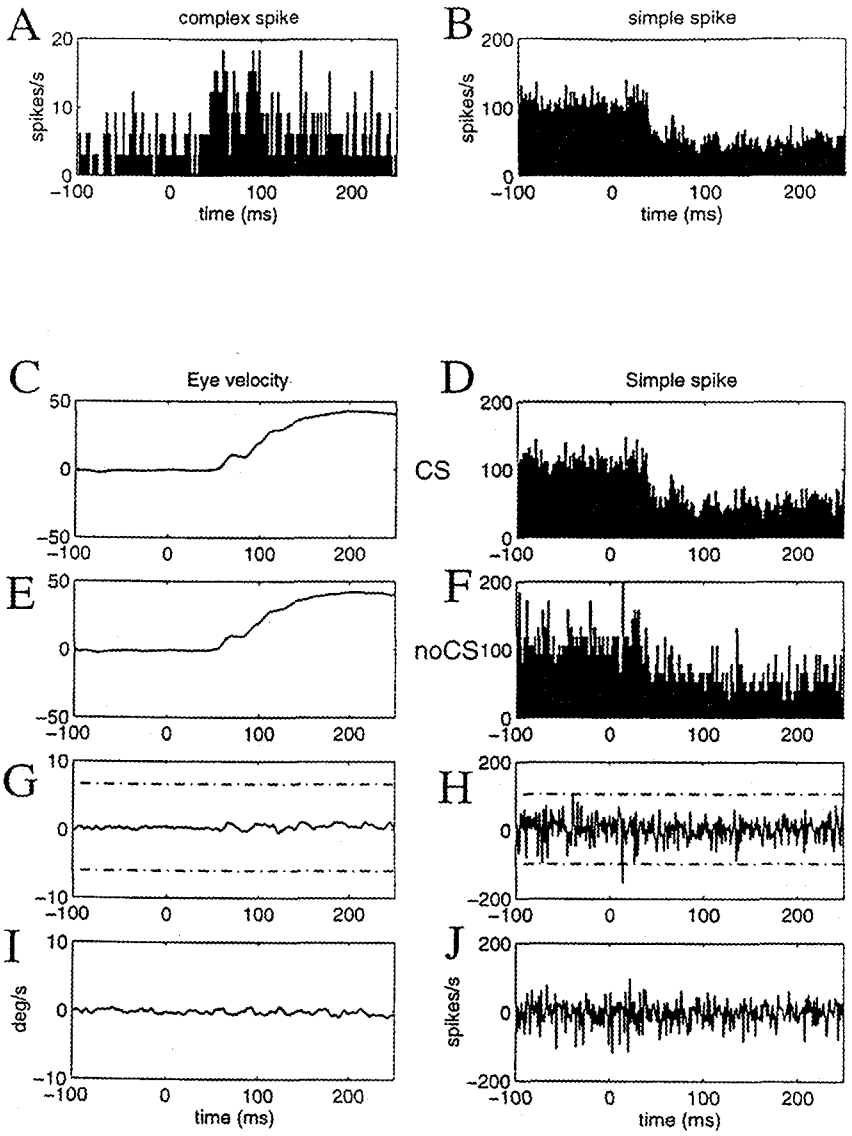

Figure 4.24: Eye velocity and SS with or without CS. CS (A) and SS (B) by upward 80 deg/s stimulus motion. Total trial number was 327. C, D shows eye velocity and SS with CS (251 trials), E, F shows eye velocity and SS without CS (76 trials). Figure G shows the difference of eye velocity between with and without CS. Figure H shows that of the SS. Broken lines in G, H shows the level mean±3SD. Figure I, J shows the result of the same analysis from the data which all of the SS and eye velocity trials were randomly shuffled.

Chapter 5

DISCUSSION

5.1 The type of information encoded by CS and the mechanism involved

Identification of the type of information and the mechanism by which that information is encoded by CS is of central importance in assessing the validity of the many current theories of climbing fiber function. CS are induced by vestibular (Ferin et al. 1971, Amat 1983; Barmack et al. 1993), visual (Maekawa and Simpson 1973; Simpson and Alley 1974; Graf et al. 1988; Stone and Lisberger 1990b; Fushiki et al. 1994), or other sensory stimuli. These data have been the basis of the common assumption that the climbing fibers convey sensory information to Purkinje cells. The present study adds new information about the motor characteristics of CS based on the following four quantitative analyses of CS firing while confirming that CS also have a sensory component.

First, the results of the present study indicate that the preferred directions of SS during OFR were close to either the vertical or horizontal axis. This is consistent with data obtained during smooth pursuit eye movements indicating that the preferred directions of SS in the VPFL were either ipsilateral or downward (Stone and Lisberger 1990a, Krauzlis and Lisberger 1996).

The preferred direction of SS and CS, and their reference frame was extensively examined in the rabbit during optokinetic responses (OKR), using a 3-D planetarium projector (Graf et al. 1988). Since we did not use the 3-D

planetarium projector stimulus system such as used in the rabbit's study (Graf et al. 1988), we could not answer the question about the spatial coordinates of CS or SS. However, Krauzlis and Lisberger (Krauzlis and Lisberger 1996) suggested that the spatial coordinates of SS in the VPFL during smooth pursuit were aligned with the coordinates of either eye muscles or semicircular canals (Krauzlis and Lisberger 1996). Their argument was based on the following data. It has been shown in lateral and frontal eyed animals, that eye muscles and semicircular canals share a similar spatial reference frame (Graf and Simpson 1981). That is, the orientations of the planes of the horizontal, anterior and posterior semicircular canals are approximately aligned with the ipsilateral horizontal lecti, vertical lecti and oblique muscles, respectively. The axes of eye muscles and semicircular canals of monkey are approximately vertical and approximately horizontal if they are projected in the front-parallel plane (Simpson et al. 1986).

In this study, since we fixed animal's head movement, sensory signals mainly came from visual system rather than from vestibular system. Furthermore, Shidara and Kawano reported that the preferred direction of SS of the Purkinje cells in the VPFL was either downward or ipsilateral, and at the site of each recording, electrical stimulation of the Purkinje cell with a single negative pulse elicited eye movement toward the preferred direction of the SS in more than one-half of the cases (Shidara and Kawano 1993). Thus, the spatial coordinate system of the SS is considered to be that of the motor commands or muscles rather than that of the vestibular input.

The medial superior temporal area of the cerebral cortex (MST) and the dorsolateral pontine nucleus (DLPN) provide visual information to the VPFL during OFR (Kawano et al. 1992, 1994a, b), and this pathway (MST-DLPN-VPFL) has been suggested to be a major sensory-motor transformation circuit (Glickstein et al. 1985; Langer et al. 1985; Tusa and Ungerleider 1988; Kawano et al. 1992, 1994a, b). Most MST and DLPN neurons showed strong directional preferences for visual stimulus motion, and when their preferred directions (directions of movement associated with the most vigorous discharges) are

plotted together in polar form it is clear that all directions of motion are represented about equally (Kawano et al. 1992, 1994a). That is, the visual coordinates for OFR are uniformly distributed in all directions. On the other hand, the spatial coordinates of the extraocular motor neurons are segregated into three channels. Thus, for OFR, the visual and motor coordinates are entirely different.

Consequently, the visual and motor components of CS can be evaluated by their spatial coordinate systems, or, in other words, their preferred directions. Approximately opposite preferred directions of visual stimulus motion for CS and SS during OFR were observed in the present study, consistent with previous data indicating that there is a reciprocal relation between SS and CS (Simpson and Alley 1974; Graf et al. 1988, De Zeeuw et al. 1995) and with data during smooth pursuit (Stone and Lisberger 1990b). The results of the present study clearly indicate that the spatial coordinates of CS during OFR were aligned with both SS and the motor command coordinates, suggesting that CS are represented in the motor-command coordinates.

Second, we examined the speed tuning properties of CS and SS during OFR. In rabbits, very low stimulus velocities (less than 1 deg/s) are optimal for evoking CS (Simpson and Alley 1974), whereas in the monkey, CS can be evoked using higher stimulus velocities; up to 50 deg/s (Noda et al. 1987). We found that CS during OFR were optimally evoked at stimulus speeds of 40 to 80 deg/s. The mean change in CS firing rate was more highly correlated with the mean eye velocity than with the mean retinal slip velocity. Furthermore, the mean change in CS firing rate was approximately a linear function of the eye velocity, but was an approximately saturating sigmoid function of the retinal slip velocity. These results also suggest that CS firing patterns include a motor component. We used a much wider range of stimulus velocities than these in a previous study of smooth pursuit eye movement (Stone and Lisberger 1990b). In that study, since target speed was relatively low (about 10 deg/s), the eye followed the step ramp motion of the stimuli quite well, and consequently the retinal slip was small. On the other hand, in our study, for the high speed

stimuli, eye movement did not perfectly follow the step ramp motion, and the gains of the OFR were significantly lower than 1 (see Figure 1 A and B); consequently a large retinal slip remained even after the initiation of the OFR (see Figure 4.7A, C and F also). In our experiment, the temporal waveforms of the eye movement and the retinal slip were markedly different, so it was possible to examine sensory and motor components separately.

Third, we compared the SS and CS temporal firing profiles. Although the CS firing rate was very low and the CS temporal firing profile was opposite in polarity to that of SS, the CS firing probability was as accurately, or more accurately, reproduced from eye movement than that of the SS. The reciprocal relationship between SS and CS was quantitatively supported by the fact that their inverse dynamics coefficients were of opposite sign and the same order of magnitude. The onset of the SS and CS modulation preceded the onset of eye movement by a similar amount indicating that CS and SS were approximately synchronous. The estimated delay in the reconstruction study was close to that of the delay (approximately 10 ms) between the electrical stimulation of Purkinje cells in the VPFL and the resultant evoked eye movement (Shidara and Kawano 1993). In smooth pursuit eye movement, the modulation of SS and CS in the VPFL is also approximately synchronized, with a delay of approximately 100 ms from the onset of stimulus motion (Stone and Lisberger 1990b), which is 50 ms longer than that for OFR. It is interesting that CS and SS exhibit synchronous modulation in the different motor behaviors.

Fourth, further examination revealed that CS had comparatively larger eye acceleration components than SS. The firing rates of the MST and DLPN neurons, which provide visual inputs to the cerebellar cortex, are not well reproduced by applying the inverse dynamics model to the eye movements in response to a wide range of stimulus velocities (Kawano et al. 1994b). This supports the widely accepted idea that these two regions convey primarily sensory information. The velocity and acceleration coefficient ratio for the eye movement model for CS was 28, which is closer to the ratio (33) for the MST and the ratio (12) for the DLPN (Takemura (in ETL Japan) et al. unpublished

observation), suggesting that , as compared with SS, CS transmit information related more to visual inputs.

The data from the present study indicate that CS possess both sensory and motor aspects, and cannot be characterized as purely sensory or purely motor in nature. Taken together, these findings indicate that the CS firing probability carries sensory error information derived from the retinal slip, but that it is already represented in the spatial and temporal frame of the dynamic motor commands. Because the Purkinje cells in the VPFL are synaptically distant from both the primary sensory and motor centers, it would a priori be very surprising if either SS or CS are purely sensory or motor in nature. The present analysis demonstrates that a more complex multi-modal relationship must exist to account for the data.

5.2 Real-time motor control by CS

The results of the present study suggest the possibility that the motor component of CS includes real-time motor commands. We discuss conditions for this to work effectively.

First, the fact that the probability of CS firing can be accurately modeled using an inverse-dynamics representation indicates that the firing probability is extracted by either spatial or temporal averaging. The signal-to-noise ratio (mean divided by standard deviation: $p/\sqrt{p(1-p)/n} = \sqrt{np/(1-p)}$) of the firing rate improves in proportion to the square root of the trial number n and the firing probability p. The rapid fluctuations in CS firing rate were relatively larger than those of SS because the CS firing probability is much smaller. There are three different ways to improve the signal-to-noise ratio for CS. First, because p increases in proportion to the width of the time bin, a short time average (over several tens of milliseconds) improves the signal-to-noise ratio while sacrificing the high temporal resolution signal. Second, if n trials are temporally averaged, the firing probability can be extracted with an accuracy proportional to $\sqrt{n}$. A third method for improving the CS signal-to-noise ratio is by spatial averaging. In terms of real-time control functions of CS, those from many Purkinje cells may be summed and spatially averaged either in the brain stem or at extraocular motor neurons and the resulting signals may represent real-time motor commands. The fact that CS have very low firing rates speaks against this possibility, as discussed further below. CS firing rates were not only very low (CS modulation was only 2 to 6% that of SS) but were completely absent in many trials, and even when CS did occur, they consisted only of a single occurrence during the period of consideration. Thus, although CS convey motor information, it appears unlikely that they contribute significantly to real-time motor control unless some strong nonlinear effects take place. For example, synchronization of the CS of many Purkinje cells may magnify the influence of CS on the downstream motor control system. However, the index of synchronization of the CS in pairs of Purkinje cells was shown to be quite small: only one order of magnitude larger than the value

expected for a pair of random independent spike trains with similar firing rate of the CS (Sugihara et al. 1993). Thus, for CS to function as effective real-time motor commands it is essential to suppose that spatial averaging occurs and that some unknown strong nonlinear summation occurs in the brain stem.

Second, if, as generally supposed, SS convey the dynamic motor commands, then CS are of the opposite sign as motor commands because the modulations of CS frequency are of opposite sign of those of SS. In other words, CS in V cells are induced by upward stimulus motion and if, like SS, they elicit downward eye movements, they would form a positive feedback loop which is harmful for real time control. The effect of CS on eye movement must, in fact, be upward if they are to form a real-time negative feedback loop to reduce the retinal slip. Three possible neural mechanisms to realize upward eye movement induced by CS will be discussed below. Direct short-term inhibition of SS by CS (Ebner and Bloedel 1981; Mano et al. 1986) is a possible sign inversion mechanism. However, in the spike trigger averaging analysis in Figure 4.23F, we showed quantitatively that this effect was too weak compared with the direct effect of CS. Thus the short-term effect on SS does not change the polarity of the net effect of CS, because this is the summation of the direct effect of CS (-2 to -6% of SS) and the short-term pause in SS firing (1% of SS) which is still negative (-1 to -5%) (and very small). The same conclusion can be reached by directly calculating how many SS were suppressed by the short-term inhibition induced by a single CS. By integrating the SS-CS net cross-correlation of Figure 12E, we estimate that only 0.11 SS were removed by a single CS ($n = 21$, in Experiment 2 and 3). Thus, the combined effect of the direct and short-term effects was 1 - 0.11 = 0.89 of the original single CS and the resulting signal was still of the opposite sign of the motor command.

The second possibility is that because of the post-inhibitory rebound burst (Llinás and Muhlethaler 1988), the net effect of CS on the recipient vestibular nuclei neurons could be an increase in firing, and CSs and SSs can be discriminated by the nuclei neurons, and the rebound excitation occurs only for CSs and not for SSs for some reasons which we do not understand. The third and

most probable possibility is that the direct excitatory pathway from the IO to the cerebellar nucleus (De Zeeuw et al. 1997b) overrides the inhibitory effect of the CSs on the cerebellar nucleus. However, this argument implies that the cerebellar cortical pathway is not useful for on-line motor control although the IO itself is effective.

Finally, the CS temporal firing profile was too phasic (i.e., too acceleration-dependent; $\frac{B}{M} = 28$) to be related to dynamic motor commands ($\frac{B}{M} = 67$). A signal must have the proper ratio of acceleration and velocity components of eye movement to function as a dynamic motor command.

In summary, the CS firing probability conveys high-frequency eye-movement-related information, and it may function as real-time motor commands during OFR, but only if some unknown strong nonlinear spatial summation of CS takes place and furthermore sign inversion occurs in the target cells only for CS (except for the short-term inhibition of SS by CS).

5.3 Interactions between CS and SS for individual cells

As discussed in the theory of CS function, possible interactions between CS and SS include short-term modulation and long-term synaptic plasticity. As discussed above, the short-term modulation was weak. In relation to long-term interactions, the following three aspects of the CS and SS firing characteristics were found to be negatively correlated on a cell-to-cell basis: (i) the optimal stimulus direction from Experiment 1, (ii) the average amount of modulation from Experiment 3, and (iii) the temporal patterns of firing probability from Experiments 2 and 3.

Four possible neural mechanisms that account for some of these correlations are as follows. First, the short-term inhibition of SS by CS may qualitatively explain all three correlations. As explained above, however, short-term inhibition was quantitatively weak and only 1 % of the SS modulation can be explained. Second, individual cell differences in size and/or input resistance may account for at least part of the second negative correlation, but does not explain the first or third negative correlation. Third, some innate anatomical connectivity between mossy fiber inputs and climbing fiber inputs may explain general SS-CS reciprocity including the first negative correlation, but does not explain the other two negative correlations. For example, if the climbing fiber inputs and the parallel fiber inputs have the same visual signal origin but the sign of one of them is inverted by an inhibitory relay center, then the general CS and SS reciprocity of directional selectivity and temporal firing profiles may be explained (Soodak et al. 1988). Because such connections are relatively non-specific at a cell-to-cell level, however, they do not explain the specific cell-to-cell negative correlations (ii) and (iii).

The fourth possible neural mechanism that may explain the three negative correlations is a long-term interaction between CS and SS. For the parallel-fiber/Purkinje-cell synapse, two types of synaptic plasticity in which the climbing fiber has a critical role are known: long-term depression, which occurs when

the climbing fiber and the parallel fiber are simultaneously active (Ito et al. 1982; Sakurai 1987; Ito 1989) and long-term potentiation, which occurs when only the parallel fiber is active (Sakurai 1987; Hirano 1991). This bi-directional change (potentiation/depression) of synaptic efficacy may occur alternately for each parallel fiber synapse. Then, on a cell-by-cell basis, this long-term interaction between CS and SS may lead to some reciprocity, that is, if the CS firing rate is high then the SS firing rate is low, and conversely if the CS firing rate is low then the SS firing rate is high for some specific characteristics of visual inputs. Thus, at least qualitatively, it is possible that all three negative correlations can be explained by a long-term interaction between CS and SS.

Finally, we give a more computationally concrete model for these negative correlations based on previous theoretical studies (Kawato and Gomi 1992a, b). Suppose that the SS temporal firing profile of each cell is acquired through the temporal averaging of the CS temporal firing profile of the same cell based on synaptic plasticity. Equation 5.1 models the above process of long-term depression and potentiation, and Equation 5.2 and 5.3 its consequence for the SS temporal profile:

$$\tau dw_i(t)/dt = -\epsilon x_i(t)\{CS(t) - CS_{\text{spont}}\} - w_i(t), \tag{5.1}$$

$$SS(t) = \sum_n w_i(t)x_i(t), \tag{5.2}$$

$$\simeq -\epsilon \sum_n \overline{x_i(t)\{CS(t) - CS_{\text{spont}}\}}x_i(t) \tag{5.3}$$

where w_i, x_i, τ, SS, CS, CS_{spont}, and the overline respectively denote the efficacy of the i-th parallel-fiber/Purkinje-cell synapse, the firing rate of the i-th parallel fiber, the time constant of synaptic plasticity, the SS and CS firing rates, the spontaneous CS firing rate, and the temporal average. Assuming linear summation of synaptic inputs in SS (Equation 5.2), and that time constant τ is much larger than the SS and CS temporal variations, Equation 5.3 predicts that SS provide an approximate sign reversed temporal average of CS on a cell-by-cell basis, because w_i becomes positive, zero, and negative if $x_i(t)$ is negatively, not, and positively temporally correlated with $CS(t) - CS_{\text{spont}}$. Considering the large cell-to-cell variability in SS and CS firing characteristics, this temporal averaging leads directly to the cell-to-cell negative corre-

lations between SS and CS. In this connection, we should consider the data in which the CSs were abolished by lesioning the inferior olive with lidocaine. The SS modulation remained, and the depth of SS modulation was unaffected (Leonard and Simpson 1986). This might be interpreted as compatible with the LTD-LTP mechanism described by Equation 5.1.

5.4 CS may convey information sufficient for motor learning

The two aspects of the experimental findings (cell-to-cell negative correlations and the sensory-motor nature of CS) become a coherent picture if it is assumed, as above, that the SS temporal firing profile is acquired through the temporal averaging of CS based on synaptic plasticity as predicted in the cerebellar feedback-error-learning model (Kawato and Gomi 1992a,b). The feedback-error-learning model specifically proposes that CS provide a copy of crude feedback motor commands, which are originally derived from sensory signals, and are used as an error signal in the acquisition of a cerebellar representation of the inverse model of a controlled object. The most unique aspect of this hypothesis is that the CS firing probability carries sensory error information derived from the retinal slip, but is already represented in the spatial and temporal frame of the dynamic motor commands so that it can directly modify SS, thus predicting both the sensory and the motor characteristics of CS. Recent computational studies (Kawato and Gomi 1992a,b) revealed that this is the essential property of the error signal if it is to be directly used to modify the motor command based on a simple heterosynaptic plasticity rule such as long-term depression and potentiation (in more computational terms, the generalized δ-rule, Rumelhart et al. 1986; Widrow-Hoff rule, 1960; the least square-error method). The following three specific predictions of the computational studies (Kawato and Gomi 1992a, b) were satisfied by the present data. The first prediction, that the spatial coordinate frame of CS is the same as that of SS was confirmed by the results of the directional tuning experiments. The second prediction was that the CS temporal firing profile is similar to that of SS; the reciprocal relationship between the SS and CS firing patterns has been shown previously in the low frequency range (Waespe and Henn 1981; Graf et al. 1988, De Zeeuw et al. 1995), and was quantitatively demonstrated in the present study in the high frequency range (several hundreds of Hz) as previously suggested (Keating and Thach 1995). The results of the present

study also support the third prediction that CS encode error signals derived from the sensory signal but are already represented temporally and spatially in motor command coordinates.

It is interesting to consider why CS (the putative error signal) remain even after sufficient learning has presumably occurred. The system controlling OFR is a dynamic feedback control system with delay. In any feedback control system, the error cannot have an immediate influence on itself, because the controlled object has inertia and any feedback loop contains time delay. Thus, the error cannot be suppressed to zero. This is obvious because, for example in OFR, the visual stimulus motion cannot be predicted beforehand and cannot be compensated for completely by the eye movement. Gomi and Kawato (1993) mathematically demonstrated that even without time delay the motor error signal is similar to the final motor command even after sufficient learning, and thus, is neither zero nor orthogonal to SS, the motor command. Time delays of approximately 40 ms, 10 ms, and 50 ms exist between the stimulus motion onset and CS, between CS and eye movement, and between stimulus motion onset and eye movement, respectively. If the CS directly influences the SS 40 ms after the onset of stimulus motion through synaptic plasticity then this change in SS leads to a change in eye movement (i.e., retinal slip) 10 ms later; 50 ms after the stimulus motion onset. The retinal slip then leads to a change in CS 40 ms later; 90 ms after the onset of stimulus motion. Thus, a CS at any particular instant can, at the earliest, influence CS 50 ms after that instant, and cannot be reduced to zero or be orthogonal to SS.

Although we needed to average discharges of Pcells over many trials (and for some purpose over several cells), this is appropriate given the likelihood that such temporo-spatial averaging will be mimicked in vivo by spatial averaging occurring in the projections from Purkinje cells to floccular target neurons. There is a quantitative histological study of numerical data on cells and on synapses in the cerebellar nuclei in the cat (Palkovits et al. 1977). Probable convergence of Purkinje axons on nuclear cells are around 860 and the number of boutons of Purkinje cells origin is 11600 per nuclear cell (Palkovits et

al. 1977). These convergence may enable the target neurons to do spatial averaging.

The present study provides evidence as to why the CS firing rate is so low. Low membrane impedance due to gap-junctions in inferior olive neurons may reduce the firing rate, but high frequency information can be preserved via spatial averaging of many inputs by electrical coupling among the inferior olive neurons (Sotelo et al. 1974).

It appears that interference by CS in real-time movement control is minimized by their ultra-low firing rate, while the high frequency information necessary for motor learning is preserved via neuronal temporal averaging (Equations 12$\sim$14).

It is interesting to note that, in studies of adaptation, OFR gains were shown to change after a small number (tens) of trials (Miles and Kawano 1986), whereas the SS temporal firing profiles observed in the present study (Figures 4.8 and 4.9) may be acquired over millions of OFRs. It remains the case that the system has not been studied while it is adapting (Miles and Kawano 1986) demonstrated that adaptation of OFR gain can be induced over the course of relatively few trials. By that experiment, we will be able to know directly how the CS will behave while they are most strongly exerting their proposed teaching function.

However, one significant factor in the present study is that perturbative "learning paradigms" such as causing the animal to learn or stimulating climbing fibers electrically were not utilized. Instead, we utilized analytical studies in normal behaving monkeys, the results of which suggest that CS represent sensory error signals that can directly modify the dynamic motor commands (SS) and reveal cell-to-cell negative correlations between the SS and CS firing characteristics, which are presumed to be acquired through life-long learning.

Bibliography

[1] Albus, J. S. A theory of cerebellar function. *Math Biosci.* 10: 25-61, 1971.

[2] Amat, J. Interaction between signals from vestibular forelimb receptors in Purkinje cells of the frog vestibulocerebellum. *Brain Res.* 278: 287-290, 1983.

[3] Andersson G. and Armstrong D. M. Complex spikes in Purkinje cells in the lateral vermis of the cat cerebellum during locomotion. *J. Physiol. (Lond.)* 385: 107-134, 1987.

[4] Barmack, N. H., Fagarson, M., Fredette, B. J., Mubnaini, E., and Shojaku, H., Activity of neurons in the beta nucleus of the inferior olive of the rabbit evoked by natural vestibular stimulation. *Exp. Brain Res.* 94: 203-215, 1993.

[5] Bell, C. C. and Grimm R. J. Discharge properties of Purkinje cells recorded on single and double micro electrodes.*J. Neurophysiol.* 32: 1044-1055, 1969.

[6] De Zeeuw, C. I., Wylie, D. R. W., Stahl, J. S., and Simpson J.I. Phase relations of Purkinje cells in the rabbit flocculus during compensatory movements. *J. Neurophysiol.* 74: 2051-2064, 1995.

[7] De Zeeuw C. I., Koekkoek S. K. E., Wylie D. R. W. and Simpson J.I. Association between dendritic laminallar bodies and complex spike synchrony in the olivocerebellar system. *J. Neurophysiol.* 77: 1747-1758, 1997a.

[8] De Zeeuw C. I., Van Alphen A. M., Hawkins R. K, and Ruigrok T. J. Climbing fiber collaterals contact neurons in the cerebellar nuclei that provide a GABAergic feedback to the inferior olive. *Neuroscience* 80: 981-986, 1997b.

[9] Ebner, T. J. and Bloedel, J. R. Role of climbing fiber afferent input in determining climbing fiber responsiveness of Purkinje cells to mossy fiber input. *J. Neurophysiol.* 45: 962-971, 1981.

[10] Ferin M., Grigorian R. A., and Strata P. Mossy and climbing fiber activation in the cat cerebellum by stimulation of the labyrinth. *Exp. Brain Res.* 12: 1-17, 1971.

[11] Fushiki, H., Sato, Y., Miura, A., and Kawasaki, T. Climbing fiber responses of Purkinje cells to retinal image movement in cat cerebellar flocculus. *J. Neurophysiol.* 71: 1336-1350, 1994.

[12] Gellman, R., Gibson, A. R., and Houk, J. C. Inferior olivary neurons in the awake cat: detection of contact and passive body displacement. *J. Neurophysiol.* 54: 40-60, 1985.

[13] Gerrits, N. M. and Voogd, J. The climbing fiber projection to the flocculus and adjacent paraflocculus in the cat. *Neuroscience* 7: 2971-2991, 1982.

[14] Gerrits, N. M. and Voogd, J. The topographical organization of climbing and mossy fiber afferents in flocculus and ventral paraflocculus in the rabbit, cat and monkey. *Exp. Brain Res. Suppl.* 17: 26-29, 1989.

[15] Gilbert, P. F. C. and Thach, W. T. Purkinje cell activity during motor learning. *Brain Res.* 128: 309-328, 1977.

[16] Glickstein, M., May, J., and Mercer, B. E. Corticopontine projection in the macaque: the distribution of labeled cortical cells after large injections of horse-radish peroxidase in the pontine nuclei. *J. Comp. Neurol.* 235: 343-359, 1985.

[17] Gomi, H. and Kawato, M. Neural network control for a closed-loop system using feedback-error-learning. *Neural Networks* 6: 933-946, 1993.

[18] Gomi, H., Shidara, M., Takemura, A., Inoue, Y., Kawano, K., and Kawato, M. Temporal Firing Patterns of Purkinje Cells in the Cerebellar Ventral Paraflocculus During Ocular Following Responses in Monkeys. I. Simple Spikes *J. Neurophysiol.* submitted, 1997.

[19] Graf, W., and Simpson, J. I. The relations between semicircular canals, the optic axis, and the extraocular muscle in lateral eyed and frontal eyed animals. *In: Progress in Oculomotor Research Developments in Neuroscience, vol 12, Edited by A. Fucks and W. Becker, Amsterdam: Elsevier/North-Holland* 411-420, 1981.

[20] Graf, W., Simpson, J. I., and Leonard, C. S. Spatial organization of visual messages of the rabbit's cerebellar flocculus. 2. complex and simple spike responses of Purkinje cells. *J. Neurophysiol.* 60: 2091-2121, 1988.

[21] Hirano, T. Depression and potentiation of the synaptic transmission between a granule cell and Purkinje cell in rat cerebellar culture. *Neurosci. Lett.* 119: 141-144, 1991.

[22] Ito, M., Sakurai, M., and Tongroach, P. Climbing fiber induced depression of both mossy fiber responsiveness and glutamate sensitivity of cerebellar Purkinje cells. *J. Physiol. (Lond.)* 324: 113-134, 1982.

[23] Ito, M. *The Cerebellum and Neural Control.* Raven Press: New York, 1984.

[24] Ito, M. Long-term depression. *Ann. Rev. Neurosci.* 12: 85-102, 1989.

[25] Judge, S. J., Richmond, B. J. and Chu, F. C. Implantation of magnetic search coils for measurement of eye position: an improved method. *Vision Res.* 20: 535-538, 1980.

[26] Julesz, B. *Foundations of Cyclopean Perception.* University of Chicago Press: London, 1971.

[27] Kawano, K., Shidara, M., and Yamane, S. Neural activity in dorsolateral pontine nucleus of alert monkey during ocular following responses. *J. Neurophysiol.* 67: 680-703, 1992.

[28] Kawano, K., Shidara, M., Watanabe, Y., and Yamane, S. Neural activity in cortical area of MST of alert monkey during ocular following responses. *J. Neurophysiol.* 71: 2305-2324, 1994a.

[29] Kawano, K., Shidara, M., Takemura, A., Inoue, Y., Gomi, H. and Kawato, M. A linear time-series regression analysis of temporal firing patterns of cerebral, pontine and cerebellar neurons during the ocular following response. *Jpn. J. Physiol.* 44: 129, 1994b.

[30] Kawano, K., Shidara, M., Takemura, A., Inoue Y., Gomi H., and Kawato M. Inverse-dynamics representation of eye movements by cerebellar Purkinje cell activity during short-latency ocular-following responses. *Ann. N. Y. Acad. Sci.* 781: 314-321, 1996.

[31] Kawato, M., Furukawa, K., and Suzuki, R. A. Hierarchical neural network model for control and learning of voluntary movement. *Biol. Cybern.* 57: 169-185, 1987.

[32] Kawato, M. and Gomi, H. The cerebellum and VOR/OKR learning models. *TINS* 15: 445-453, 1992a.

[33] Kawato, M. and Gomi, H. A computational model of four regions of the cerebellum based on feedback-error-learning. *Biol. Cybern.* 68: 95-103, 1992b.

[34] Kawato, M. Analysis of neural firing frequency by a generalized linear model. *Tech. Rep. of IEICE* NC95-33: 31-38, 1995.

[35] Keating, J. G. and Thach, W. T. Nonclock behavior of inferior olive neurons: interspike intervals of Purkinje cell complex spike discharge in the awake behaving monkey is random. *J. Neurophysiol.* 73: 1329-1340, 1995.

[36] Keller, E. L. Accommodative vergence in the alert monkey motor unit analysis. *Vision Res.* 13: 1565-1575, 1973.

[37] Kobayashi, Y., Kawano, K., and Kawato, M. The analysis of firing frequency of spike discharges using a generalized linear model (model examination). *Tech. Rep. of IEICE* NC95-34: 39-46, 1995.

[38] Krauzlis, R. J. and Lisberger, S. G. Directional organization of eye movement and visual signals in the floccular lobe of the monkey cerebellum. *Exp. Brain Res.* 109: 289-302, 1996.

[39] Langer, T., Fuchs, A. F., Scudder, C. A., and Chubb, M. C. Afferents to the flocculus of the cerebellum in the rhesus macaque as revealed by retrograde transport of horseradish peroxidase. *J. Comp. Neurol.* 235: 1-25, 1985.

[40] Leonard, C. S. and Simpson, J. I. Simple spike modulation of floccular Purkinje cells during the reversible blockage of their climbing fiber afferents. *In Keller, E.L. and Zee, D.S. (Eds) Advances in the Biosciences 57: Adaptive processes in visual and oculomotor systems. Pergamon Press Oxford*: 321-328, 1986.

[41] Lisberger, S. G. and Westbrook, L. E. Properties of visual inputs that initiate horizontal smooth pursuit eye movements in monkeys. *J. Neurosci.* 5: 1662-1673, 1985.

[42] Llinás, R., Baker, R., and Sotelo, C. Electrotonic coupling between neurons in cat inferior olive. *J. Neurophysiol.* 37: 560-571, 1974.

[43] Llinás, R., and Mühlethaler M. Electrophysiology of guinea-pig cerebellar nuclear cells in vitro brain stem-cerebellar preparation. *J. Physiol. (London)* 404: 241-258, 1988.

[44] Lou, J. S. and Bloedel, J. R. The responses of simultaneously recorded Purkinje cells to the perturbations of the step cycle in the walking fer-

ret: a study using a new analytical method-the real time post synaptic response (RTPR). *Brain Res.* 365: 340-344, 1986.

[45] Lou, J. S. and Bloedel, J. R. Responses of sagittally aligned Purkinje cells during perturbed locomotion: synchronous activation of climbing fiber inputs. *J. Neurophysiol.* 68: 570-580, 1992.

[46] Maekawa, K. and Simpson, J. I. Climbing fiber responses evoked in vestibulo-cerebellum of rabbit from visual system. *J. Neurophysiol.* 36: 649-666, 1973.

[47] Mano, N., Kanazawa, I., and Yamamoto, K. Complex-spike activity of cerebellar Purkinje cells related to wrist tracking movement in monkey. *J. Neurophysiol.* 56: 137-158, 1986.

[48] Marr, D. A theory of cerebellar cortex. *J. Physiol.* 202: 437-470, 1969.

[49] McCullagh, P. and Nelder, F. R. S. *Generalized Linear Models.* Chapman Hall: London, 1989.

[50] Miles, F. A., Kawano, K., and Optican, L. M. Short-latency ocular following responses of monkey. I. dependence on temporospatial properties of visual input. *J. Neurophysiol.* 56: 1321-1354, 1986.

[51] Miles, F. A. and Kawano, K. Short-latency ocular following responses of monkey. III. plasticity. *J. Neurophysiol.* 56: 1381-1396, 1986.

[52] Noda, H., Warabi, T., and Ohno, M. Response properties and visual receptive fields of climbing and mossy fibers terminating in the flocculus of the monkey. *Exp. Neurol.* 95: 455-471, 1987.

[53] Ojakangas, C. L. and Ebner T. J. Purkinje cell complex spike activity during voluntary motor learning: relationship to kinematics. *J. Neurophysiol.* 72: 2617-2630, 1994.

[54] Oscarsson O. Functional organization of olivary projection to the cerebellar anterior lobe. In *The inferior olive nucleus: Anatomy and Physiology* ed. Courvile J, C de Montigny and Lamarre Y. Raven: New York, 1980.

[55] Palkovits M., Mezey E., Hamori J., and Szentagothai J. Quantitative histological analysis of the cerebellar nuclei in the cat. I. numerical data on cells and on synapses. *Exp. Brain Res.* 28: 189-209, 1977.

[56] Perkel, D. H., Gerstein, G. L., and Moore, G. P. Neuronal spike trains and stochastic point processes. II. simultaneous spike train. *Biophys. J.* 7: 419-440, 1967.

[57] Ron, S. and Robinson, D. A. Eye movements evoked by cerebellar stimulation in the alert monkey. *J. Neurophysiol.* 36: 1004-1022, 1973.

[58] Rumelhart, D. E. and McClelland, J. L. *Parallel Distributed Processing: Explorations in the Microstructure of Cognition, 1, 2.* MIT Press: Cambridge Massachusetts, 1986.

[59] Rushmer, D. S., Roberts, W. J., and Augter, G. K. Climbing fiber responses of cerebellar Purkinje cells to passive movement of the cat forepaw. *Brain Res.* 106: 1-20, 1976.

[60] Sakurai, M. Synaptic modification of parallel fiber-Purkinje cell transmission in vitro guinea-pig cerebellar slices. *J. Physiol. (Lond.)* 394: 463-480, 1987.

[61] Sato, Y., Miura, A., Fushiki, H., and Kawasaki, T. Short-term modulation of cerebellar Purkinje cell activity after spontaneous climbing fiber input. *J. Neurophysiol.* 68: 2051-2062, 1992.

[62] Shidara, M. and Kawano, K. Role of Purkinje cells in the ventral paraflocculus in short-latency ocular following responses. *Exp. Brain Res.* 93: 185-195, 1993.

[63] Shidara, M., Kawano, K., Gomi, H., and Kawato, M. Inverse-dynamics encoding of eye movements of Purkinje cells in the cerebellum. *Nature* 365: 50-52, 1993.

[64] Simpson, J. I. and Alley, K. E. Visual climbing fiber input to rabbit vestibulo-cerebellum: a source of direction-specific information. *Brain Res.* 82: 302-308, 1974.

[65] Simpson, J. Rudinger, D., Reisine, H., Henn, V. Geometry of extraocular eye muscles of the rhesus monkey. *Soc. Neurosci. Abstr.* 12: 1186, 1986.

[66] Simpson, J. I., Wylie, D. R., and De Zeeuw, C. I. On climbing fiber signals and their consequence(s). *Behavioral and Brain Sciences* 19: 384-398, 1996.

[67] Soodak, R. E. , Croner, L. J., and Graf, W. Development of the optokinetic reference frame of floccular Purkinje cells in rabbit. *Soc. Neurosci. Abstr.* 14: 758, 1988

[68] Sotelo, C., Llinás, R., and Baker, R. Structural study of inferior olivary nucleus of the cat: morphological correlates of electrotonic coupling. *J. Neurophysiol.* 37: 541-559 ,1974

[69] Stone, L. S. and Lisberger, S. G. Visual responses of Purkinje cells in the cerebellar flocculus during smooth-pursuit eye movements in monkeys I. simple spikes. *J. Neurophysiol.* 63: 1241-1261, 1990a.

[70] Stone, L. S. and Lisberger, S. G. Visual responses of Purkinje cells in the cerebellar flocculus during smooth-pursuit eye movements in monkeys II. complex spikes. *J. Neurophysiol.* 63: 1262-1275, 1990b.

[71] Sugihara, I., Lang, E. J., and Llinas, R. Uniform olivocerebellar conduction time underlies Purkinje cell complex spike synchronicity in the rat cerebellum. *J. Physiol. (London)* 470: 243-271, 1993.

[72] Thach, W. T. Discharge of cerebellar neurons during rapidly alternating arm movement in the monkey *J. Neurophysiol.* 31: 785-797, 1968.

[73] Toyama, K., Kimura, M., and Tanaka, K. Cross-correlation analyses of interneuronal connectivity in cat visual cortex. *J. Neurophysiol.* 46: 191-201, 1981.

[74] Tusa, R. J. and Ungerleider, L. G. Fiber pathways of cortical areas mediation smooth pursuit eye movements in monkeys. *Ann. Neurol.* 23: 174-183, 1988.

[75] Udo, M., Kamei, H., Matukawa, K., and Oda, Y. Simple and complex spike activities of Purkinje cells during locomotion in the cerebellar vermal zone of decerebrate cats. *Exp. Brain Res.* 41: 292-300, 1981.

[76] Waespe, W. and Henn, V. Visual-vestibular interaction in the flocculus of the alert monkey. I. input activity. *Exp. Brain Res.* 43: 349-360, 1981.

[77] Welsh, J. P., Lang, J. E., Sugihara, I., and Llinas, R. Dynamic organization of motor control within the olivocerebellar system. *Nature* 374: 453-457, 1995.

[78] Widrow, B. and Hoff, M. E. Adaptive switching circuits. *WESCON Conv. Rec.* IV: 96-104, 1960.

[79] Wylie, D. R., DeZeeuw, C. I., and Simpson, J. I. Temporal relations of the complex spike activity of Purkinje cell pairs in the vestibulocerebellum of rabbits. *J. Neurosci.* 15: 2875-2887, 1995.

Acknowledgments

I am grateful to Dr. Mitsuo Kawato and Dr. Kenji Kawano for their suggestions and their kind help. I wish to thank Dr. F. A. Miles for help with manuscript and S. M. Highstein for very helpful criticisms. I thank Dr. Fujio Murakami and Dr. Tadashi Isa for their encouragements during this work.

I thank Dr. Hiroaki Gomi, Dr. Kenji Yamamoto, Dr. Shigeru Kitazawa and Dr. Hiroshi Aizawa for discussions, and Mr. Toshinori Yoshioka for many technical suppots, Dr. Aya Takemura, Dr. Yuka Inoue, Dr. Toshihiro Kitama and Dr. Munetaka Shidara for help during experiments.

I also thank Dr. Yoshikazu Shinoda, Dr. Keisuke Toyama, Dr. Yo-ichi Tohkura, Dr. Makoto Taketani, Dr. Hirokazu Sugihara and Dr. Tadayasu Mitsumata for their encouragement during this work. I also thank M s Mieko Namba and Miss Chika Suzuki for help with figures.

This work was supported by ATR grant, CREST-JST and HFSP. Present address of Y. Kobayashi, Department of Integrative Physiology, National Institute for Physiological Sciences, Myodaiji, Okazaki, Aichi 444-8585, Japan

List of papers

Manuscripts

1. Kobayashi Y, Kawano K, Takemura A, Inoue Y, Kitama T, Gomi H, Kawato M: Temporal Firing Patterns of Purkinje Cells in the Cerebellar Ventral Paraflocculus During Ocular Following Responses in Monkeys. II. Complex Spikes. *J. Neurophysiol.*, in press (1998).

2. Yamamoto K, Kobayashi Y, Kawano K, Takemura A, Kawato M : A mathematical model that reproduces vertical ocular following responses from visual stimuli by reproducing by simple spike firing frequency of Purkinje cells in the cerebellum. *Neurosci. Res* **29**: 161-169 (1997)

3. Murakami F, Kobayashi Y, Uratani T, Tamada A: Individual corticorubral neurons project bilaterally during postnatal development and following early contralateral cortical lesions. *Exp. Brain Res.* **96**: 181-193 (1993)

4. Song WJ, Kobayashi Y, Murakami F: An electrophysiological study of a transient ipsilateral interpositorubral projection in neonatal cats. *Exp. Brain Res.* **92**: 399-406 (1993)

International conferences

1. Murakami F, Kobayashi Y, Uratani T, Tamada A: Crossed corticorubtral axons in newborn kittens and hemispherectomized kittens are collaterals of uncrossed axons. *Soc.Neurosci.Abstr.***17**: 765 (1991)

2. Kobayashi Y, Sugihara H, Mitsumata T, Toyama K Development and plasticity of neural connectivities between aggregates of rat visual cortical cells cultured in a multielectrode dish. *Soc.Neurosci.Abstr.* **19**: 27.7, 42 (1993)

3. Kamei A, Sugihara H, Kobayashi Y, Taketani M, Tomiyama K, Merzhanova G, Yamamoto N, Toyama K: Development of neural transmission in rat visual cortex studied by organotipic cultures grown on multielectrode dishes. *Soc. Nerosci. Abstr.* **20**: 466 (1994)

4. Kobayashi Y, Kawato M, Kawano K, Inoue Y, Shidara M, Gomi H: Complex-spike Activity of Purkinje Cells in Monkey Cerebellar Ventral Paraflocculus during Ocular Following Response.*Fourth IBRO World Congress of Neuroscience, Annual Meeting Abstracts* **D5.4**: 327 (1995)

5. Kobayashi Y, Kawato M, Gomi H, Kawano K, Shidara M, Inoue Y : Inverse-Dynamics Representation of Complex Spike Discharges of Purkinje Cells in Monkey Cerebellar Ventral Paraflocculus during Ocular Following Responses. *Soc.Neurosci.Abstr.* **21**:61.6, 140 (1995)

6. Kawato M, Kobayashi Y, Kawano K, Takemura A, Inoue Y, T KItama, H Gomi: Cell-to-Cell Negative Correlations between the Simple Spike and the Complex Spike Firing Characteristics of Individual Purkinje Cells. *Soc.Neurosci.Abstr.* **23**:511.9, 1299 (1997)

7. Kobayashi Y, Kawano K, Takemura A, Inoue Y, T Kitama, H Gomi, Kawato M : Temporal firing patterns of Purkinje Cells Cerebellar Ventral Paraflocculus during ocular following Responses in monkeys. *Soc.Neurosci.Abstr.* **23**:511.10, 1299 (1997)

8. Aizawa H, Kobayashi Y, Yamamoto M , Isa T : Modification of saccadic eye movements by acetylchline-ralated substances injected into monkey superior colliculus. *Soc.Neurosci.Abstr.* **23**:510.16, 1297 (1997)

9. Yamamoto K, Kobayashi Y, Kawano K, Takemura A, Kawato M : A simulation system for vertical ocular following responses with simple

spike firing rate of Purkinje cells in the cerebellum. *Soc.Neurosci.Abstr.* **23**:609.6, 1299 (1997)

10. Aizawa H, Kobayashi Y, Yamamoto M and Isa T: Modification of the initiation of saccadeic eye movements by micro-injection of acetylchline-ralated substances into monkey superior colliculus. *NCM meeting 98* (1998)

Domestic conferences

1. Song WJ, Kobayashi Y, Yamazaki M, Murakami F Regressive aberrant projections in the developing CNS of mammalian are functional *Neurosci. Res.(Supple)***11**:34 (1990)

2. Kobayashi Y, Sugihara H, Kamei A, Tomiyama K, Yamamoto N, Merzhanoya G, Toyama K: Developmental study of neural connectivities in rat visual cortical cultures grown in multielectrode dishes.*J. Phisiol. (Japan) supple* **44**: S181 (1994)

Books

1. Kawano K, Takemura A, Inoue Y, Kitama T, Kobayashi Y, Mustari M: Visual inputs to cerebellar ventral paraflocculus during ocular following responses. Progress in Brain Research "Extrageniculostriate Mechanisms underlying Visually-Guided Orientation Behavior" Stein et al.(Eds) Elsevier, Amsterdam (1996)